4-2012

A Numerical Investigation of Two Phase Solar-Collector Pipe

Seyyed Hashem Abedini
University of Nebraska – Lincoln, sabedini@unomaha.edu

A Numerical Investigation of Two Phase Solar-Collector Pipe

By

Seyyed Hashem Abedini

A THESIS

Presented to the Faculty of

The Graduate College at the University of Nebraska

In Partial Fulfillment of Requirements

For the Degree of Master of Science

Major: Architectural Engineering

Under the Supervision of Professor Siu-Kit Lau

Lincoln, Nebraska

May, 2012

A Numerical Investigation of Two Phase Solar-Collector Pipe

Seyyed Hashem Abedini, M.S.

University of Nebraska, 2012

Advisor: Siu Kit Lau

In the United States, major portions of the annual electrical and primary energy are consumed for buildings. To help reduce the energy consumption of non-renewable energy sources, this study investigates a new technology for harvesting solar energy using a boiling-condensing cycle with water in a solar collector. The fluid circulation is under natural forced convection. A solar collector is made of a black lacquer copper with 2 meters in length is used. The design of the system is presented to simulate heat transfer rate in a cold climate an average daily solar irradiation of 4.5kWh/m^2/day, e.g. for Omaha Nebraska. The tube surface temperature is calculated based on specified ambient temperature and solar radiation, i.e. 302.6K.

A constant tube surface temperature is considered in this simulation-based study. The solar collector will not freeze since this system uses the lower pressure inside the tube. The correlations for the heat transfer coefficients in non-boiling and boiling regions are presented. This study analyzes the heat transfer development of a single phase flow and two-phase flow boiling process in different regions such as subcooled flow region, saturated flow boiling region and vapor region in various pressures. This research investigates how to maximize heat transfer in a single vertical tube. The proper subcooled

flow region in the overall tube length and also a specific pressure are optimized and estimated to calculate the maximum total heat transfer rate in a solar collector. It is concluded that the maximum heat transfer rate will be obtained when the vapor region is minimized and the subcooled and saturation region are maximized in overall tube length.

DEDICATION

I dedicate this thesis first to my wonderful wife Mariam Rahmani for all her love and support during the years my study. I would also like to dedicate this thesis to my lovely daughter, Niki, for bringing joy and happiness to our life.

AUTHOR'S ACKNOWLEDGEMENTS

I would like to express my special thanks and gratitude to my supervisor, Dr. Siu-Kit Lau, whose encouragement, guidance and support from the start to the finish of thesis project enabled me to develop an understanding of the subject of the thesis. I am really thankful to him.

I would also like to sincerely thank my committee members, Dr. Junke Guo and Dr. Alahmad Moe, for their instructions and help. Thank you all.

It is my pleasure to give a special thank you to Dr. Gren Yuill, who assisted me with selecting major, as well as for his kindness and patience in being my first advisor at the university.

I owe many thanks to my great friends, Mr. Carl Hart, Mr. Bob Deford, Ms. Nargess Tahmasbi, and my dear wife, Mariam Rahmani, who helped and supported me during doing this project.

Lastly, I offer my regards and blessings to all of those who supported me during the completion of the project.

TABLE OF CONTENTS

LIST OF TABLES

LIST OF FIGURES

NOMENCLATURE

^{o}F	Degree Fahrenheit
DHW	Domestic Hot Water
℃	Degree Celsius
K	Degree Kelvin
T	Temperature [K]
T_s	Tube Surface Temperature [K]
T_f	Liquid Temperature [K]
T_{sat}	Saturation Temperature [K]
m	Meter
D	Tube Inner Diameter[m]
L	Tube Length [m]
h_{lo}	Single- Phase Heat Transfer Coefficient [W/m^{2}K]
m^2	Squer Meter
W	Watt [J/s]
J	Joule
S	Second
ONB	Onset of Nucleat Boiling
FDB	Fully Developed Boiling
NVG	Net Vapor Generation
h	Heat Transfer Coefficient [W/m^{2}K]
$\overline{x}$	Vapor Quality
G	Mass Flux [kg/sm^2]

kg	Kilogram
q	Heat Flux [W/m^2]
DNB	Departure from Nucleate Boiling
CHF	Critical Heat Flux [W/m^2]
Bo*	Modified Boiling Number
ρ_l	Liquid Density [kg/m^3]
m^3	Cubic Meter
ρ_g	Vapor Density [kg/m^3]
ρ_l/ρ_g	Density Ratio
Bo	Boiling Number
h_{TP}	Two-Phase Heat Transfer Coefficient [W/m^{2}K]
F_{fl}	Fluid-Dependent Parameter
T_m	Liquid Mean Temperature [K]
Re_D	Reynolds Number
μ_l	Viscosity of Liquid [Ns/m^2]
μ_g	Viscosity of Vapor [Ns/m^2]
$\dot{m}$	Mass Flow Rate [kg/s]
Nu_D	Nusselt Number
Pr	Prandtl Number
ν	Momentum Diffusivity [m2/s]
α	Thermal Diffusivity [m2/s]
f	Liquid Friction Factor
$c_{p,f}$	Specific Heat [kJ/kgK]

kJ	Kilo Joule
$\overline{h_{lo}}$	Average Convection Heat Transfer Coefficient [W/m^{2}K]
z	Axial Position of The Tube [m]
i	Inlet
$\overline{k_l}$	Average Thermal Conductivity [W/mK]
NBD	Nucleate Boiling Dominant
CBD	Convective Boiling Dominant
$(h_{TP})_{NBD}$	Heat Transfer Coefficient of Nucleate Boiling Dominant Region [W/m^{2}K]
$(h_{TP})_{CBD}$	Heat Transfer Coefficient of Convective Boiling Dominant Region [W/m^{2}K]
Max	Maximum
$f_2(Fr_l)$	The Stratification Parameter
h_{fg}	Heat of Vaporization [kJ/kg]
A	Cross-Sectional Area of Tube [m^2]
h_g	Single-Phase Vapor Heat Transfer Coefficient [W/m^{2}K]
k_g	Vapor Thermal Conductivity [W/mK]
u	Velocity of Liquid [m/s]
A_s	Tube Area [m^2]
$\dot{Q}$	Total Heat Transfer Rate [W]
$(\frac{q}{A})_{sun}$	Solar Flux [W/m^2]
α_{sun}	Absorptivity of Solar Radiation
$\alpha_{low\ temp}$	Absorptivity for Low-Temperature Radiation
σ	Estefan-Boltzmann Constant [W/m^{2}K^4]

T_{surr} Surrounding Temperature [K]

Chapter 1

1. Introduction

1.1 Motivation

This chapter presents the motivation of the research tackled in this thesis. The chapter also provides the main objectives of the research and outlines each chapter.

This research aims to develop a high-efficiency technology for harvesting solar energy using a boiling-condensing cycle in a domestic hot water system. Buildings dominate energy consumption in the U.S. They consume 40% of primary energy and 70% of electric energy. The U.S. Department of Energy (DOE) has adapted Zero-Net Energy Buildings (ZNEB) as a strategic goal in their efforts aimed at energy efficiency and sustainability. DOE plans to achieve ZNEB by (1) reducing the energy used by housing by an average 30% to 90% through improved energy systems efficiency and conservation, and (2) compensating the rest of the energy use by on-site renewable energy generation (DOE, 2009). However, the ability to cost-effectively harvest on-site renewable energy in environmentally friendly and safe manners is one of the primary barriers to an effective renewable energy solution. This problem is particularly important in the Midwest and Western areas of the United State because of the low population density and the limited availability of transmission lines.

Besides achieving energy use reduction and system efficiency improvement, the success of the strategic goal of ZNEB relies greatly on offsetting part of the energy usage through on-site renewable energy generation. Solar domestic water heating systems are

generally efficient and cost-effective in climates where freeze protection is not required. In regions where freezing occurs, these systems become more complex and expensive. The proposed system in the present study is an innovative solar hot water system that uses a boiling-condensing cycle. Maximized heat transfer in the solar collectors can be achieved by forced convection boiling in two-phase flow. This system has the advantages of easy freeze protection and no pumping or control system requirements. The goal of this study is to develop a solar hot water system to maximize the efficiency and effectiveness of renewable energy usage, which can reduce non-renewable energy usage for hot water heating.

The performance efficiency and cost-effectiveness of solar water heating is generally much higher than that of photovoltaic systems. The heat pipe, where heat absorbed at one end of a pipe by vaporization of the fluid can be released at the other end by condensation of the vapor, is a highly efficient device for heat transmission. It has advantages of transferring heat at high rates over considerable distances, with extremely small temperature drop between the evaporator section (heat region) and the condenser section (cooled region) of the pipe. However, current work on such systems has largely centered on using refrigerants as the working fluid. This means that a double-walled heat exchanger must be used to comply with the regulation of food safety in most states in the U.S and in the countries, which dramatically degrades the system performance and cost efficiency. This study will develop a solar collector system using a boiling-condensing cycle with water as the working fluid in order to significantly improve the system performance and applicability. Compared with the conventional solar water heating system, the system has the advantages of operating as a thermal diode (when the collector

temperature is less than the storage water temperature, the heat energy will not be lost from storage tanks); good resistance against corrosion; elimination of contamination of potable water; easy freeze protection; and no pumping or control system requirements. This latter point means that the system will not require an electrical connection. This study aims to develop an entirely new solar hot water system to collect and store the solar energy. Emphasis will be placed on optimizing a solar hot water system using the boiling-condensing cycle for harvesting solar energy.

Solar domestic water heating systems can be economical in climates where the lowest temperatures in winter will not freeze the water in the collectors. Where the temperature may drop below freezing, they are not generally economical. This is partly because of the cost of freeze protection. The proposed system in this study avoids these difficulties by a solar collector system that operates at a low enough pressure. The water in it will boil at the temperatures that can be achieved under solar irradiation as shown in Figure 1.1. The water vapor (steam) will then flow from the top of the collector to a vapor-release drum and a heat exchanger in the domestic hot water (DHW) system. The vapor-release drum, which is connected between the solar collector and the heat exchanger, is used to assure that vapor always remains in the inlet of the heat exchanger during the normal operation of the system; then water vapor will condense, giving off its heat to the water. The condensate will then flow back into the bottom of the solar collector to be boiled and circulated again.

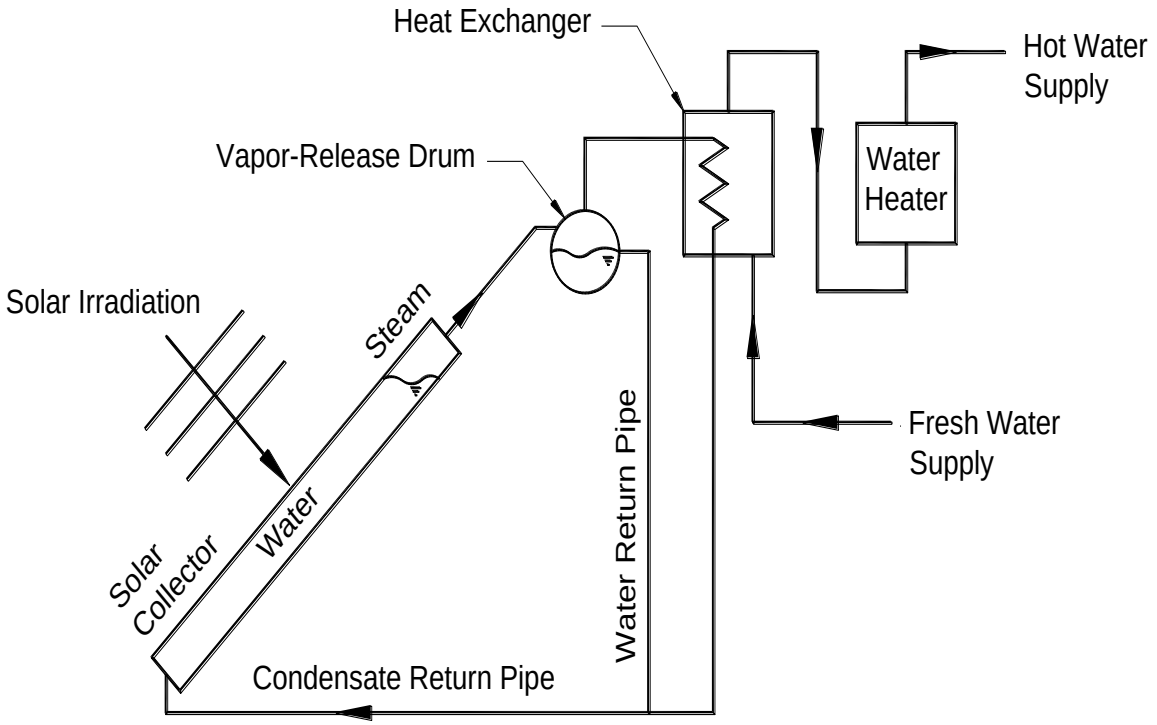

Figure 1.1 Schematic diagram of the proposed solar hot water system

The heat transfer coefficients for boiling and condensation heat transfer are far higher (20 to 100 times higher) than for single phase convective heat transfer. Therefore the solar collectors will operate more efficiently, as will the heat exchanger between the solar loop and the potable water. The amount of water circulated can be far less than in conventional systems because the enthalpy of evaporation is so much higher than the sensible enthalpy changes that occur when water is heated and cooled. The enthalpy change that occurs when water is boiled is 50 times higher than when water is heated by 20 ^{o}F (a reasonable temperature difference for a standard solar collector).

Previous studies of related concepts have focused on using refrigerants (R410A, R407C, R134a and R11) as working fluids (Esen and Esen, 2005; Joudi *et al*., 1999).

Though Anderson *et al*. (2009) and Hwang *et al*. (2007) showed the application of the water heat pipe for extreme environments in the Moon and the Mars, the wick and titanium heat pipe are not necessary in domestic water heating. The study most relevant to the present study (Hussein, 2007) only showed the performance of components in a particular climate and configuration. A system is proposed very different from his, because it is maximized heat transfer in the solar collectors by optimization of forced convection boiling in two-phase flow. The proposed system can be operated in one of two ways, using natural circulation or using a pump. In the natural circulation system the bottom of the heat exchanger in the DHW system is above the top of the solar collectors. Water boils in the solar collectors, the steam flows to the heat exchanger and condenses, and the condensate returns to the solar collectors due to gravity. This system is cheap and simple, with no moving parts and no requirement for controls or for an electricity connection.

In some situations, it isn't practical to arrange the solar collectors and the DHW system so that gravity return is possible. In that case, a pump can be used. However, the very low flow rate required means that the pump can be much smaller, reducing the cost of the pump, and its power consumption. Of course, using a pump means that an electrical connection would be required.

The main advantage of the proposed low pressure system is freeze protection. Because the system is only partly filled with water, ice can form in the solar collector tubing without rupturing. Ice forming in a partially-filled tube will simply squeeze along the tube as it expands. (This mechanism has been tested by Dr. Siu-Kit Lau, Dr. Gren Yuill and Mr. Carl Hart of the University of Nebraska-Lincoln, and freezing did not

rupture the tubing.) Eliminating the need for freeze protection greatly reduces the cost of a solar DHW heating system and/or increases its efficiency.

1.2 Goals

The rationale of the study is to establish an optimal and integrated domestic hot water system based on a boiling-condensing cycle to maximize high heat transfer coefficient and total heat transfer rate in a the solar collector tube. Also one of the goals of the thesis is to understand the two-phase flow boiling process inside the solar collector tube and its behavior under different conditions with various factors (e.g. pressure and tube size). The study is preferred to maximize heat transfer and optimize the overall system performance with regarding to existing condition such as average surrounding temperature at cold and warm months and average solar irradiation at different territories.

1.3 Structure of Thesis

The next chapter presents the literature review of this study. The chapter 3 is focused on methodologies of this research. The chapter 4 discusses heat transfer coefficients. The chapter 5 focuses on optimization estimation and energy performance of system design. The chapter 6 concentrates on conclusions and recommendations for future work.

Chapter 2

2. Literature Review

2.1 Introduction

There are several research works have been done regarding to process of flow boiling of a liquid. The process of liquid flow boiling in heated confined passage is discussed in various applications, for instance, steam generators in power plants, evaporators in refrigeration, and air conditioning equipment (Kandlikar *et al*., 1999). The heat transfer related from changing single-phase liquid to two-phase flow boiling in a vertical heating pipe is an important topic in evaporators in the process industry for mechanical, chemical, petrochemical and hydrometallurgical performances (Saffari and Ghobadi, 2010). A boiling-condensing cycle in a domestic hot water system can also be applied in harvesting solar energy (Wangee Chun *et al*., 1999).

The seminal literatures on flow boiling will be reviewed in this chapter. In the second section of this chapter, forming different regions of water flow boiling in a vertical tube will be explained. The third section will present some of the background works related to the development of subcooled, saturated, and vapor boiling regions.

2.2 Regions of Flow Boiling

Figure 2.1 shows more details about various regions of flow boiling (Kandlikar *et al*., 1999). Heat transfer to a liquid flowing inside a tube is by single-phase heat transfer as long as the temperatures of the liquid, T_f, and the wall, T_w, are less than the saturation temperature of the liquid, T_{sat}, at the local pressure from the inlet (location A). In the following sections of this dissertation T_s is used instead of T_w, the subcooled liquid heat-

transfer is initially transferred through single-phase forced convection. Farther downstream in the tube (upward of the tube in Figure 2.1), the wall temperature surpasses the local saturation temperature of the liquid, T_{sat}, at location C and vaporization is started in the subcooled flow boiling region. The boiling process in the subcooled flow significantly improves the heat transfer rate the single-phase value, which will be shown in later in this section.

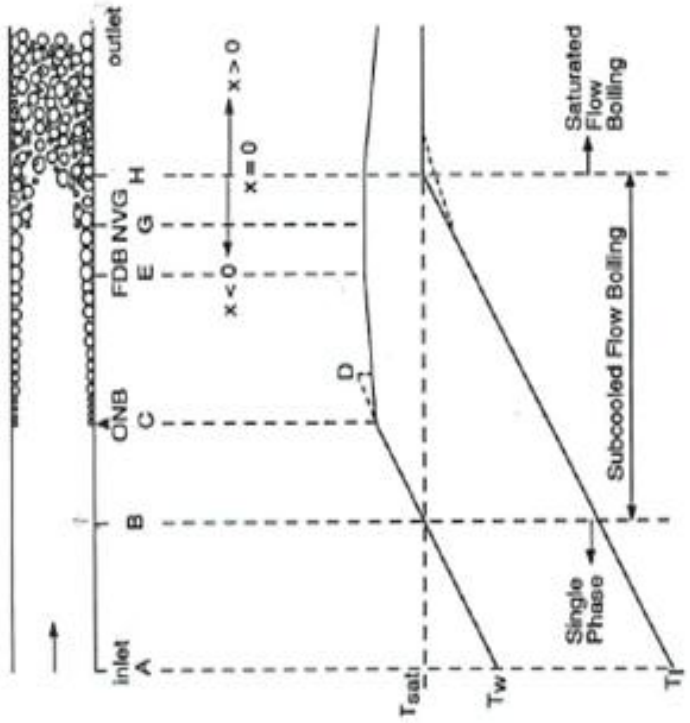

Figure 2.1 Flow boiling process in subcooled area (Kandlikar *et al.*, 1999)

In a condition of constant heat flux, the bulk water temperature and the wall temperature vary along throughout the tube. For a circular tube of diameter *D*, the water temperature variation in the flow direction in the non-boiling region (before location C) can be extracted from an energy balance over the tube lenght, *L*. In the single-phase

region, the heat transfer coefficient, h_{lo}, is almost constant, and the wall temperature, T_s, linearly increases and its curve is parallel to that of the water tempreature, T_f, along the tube as shown in Figure 2.1. At location B, the wall temperature, T_s, would reach the saturation temperature of the liquid, T_{sat} . A certain amount of heat energy on the wall is required to create vapour cavities on the suface of the tube wall. At location C, the first bubbles appear on the wall, which is considered the onset of nucleat boiling or ONB. The wall temperature starts to level off as more bubbles are created beyond ONB. Since more nucleation sites are activated farther downstream, the contribution to heat transfer from nucleate boiling will increase and single-phase convective contribution will disappear. This area is called partial boiling region. At location E, the convective contribution becomes unimportant and the fully developed boiling (FDB) will appear. The wall temperature stays constant in the FDB area until a point where the convective effects become more important due to the two-phase flow. The bubbles created at the wall instantly following ONB cannot grow because of the condensation that occures at the bubble surface exposed to the subcooled liquid flow. A slim layer of bubles is shaped on the wall surface. As the liquid water temperature rises in the flow direction, more bubbles will be formed with increasing bubble size and decreasing subcooling region. These bubbles finally separate from the wall and flow toward the liquid core at the location G. Some bubbles condense along the way. Location G is known as the point of net vapor generation (NVG). The vapor after location NVG is at the saturation temperature (Kandlikar *et al*., 1999). The the state of a subcooled liquid is defined in terms of an equilibrim "quality" based on the liquid enthalpy relative to its saturation state at the same pressure. The quality is used as an independent variable to represent the fluid state

along with an evaporator tube. The negative quality condition is referred to as the subcooled region and the positive quality is referred to as the saturated region. With increasing heat along with the tube, a saturation condition under thermodynamic equilibrium will be reached at location *H* in Figure 2.1. Because of non-equilibrium conditions, the real liquid temperature is actually lower than the saturation temperature as shown by a dashed line in Figure 2.1 (Kandlikar *et al*., 1999).

Figure 2.2 is a more comprehensive view of flow boiling regimes rather than Figure 2.1 that only shows the subcooled flow region. As shown in Figure 2.2 (Incropera et al., 2006), if the wall temperature surpasses the local saturation temperature, saturated flow boiling would be created and vapor quality will be between zero and one. The heat transfer coefficient, *h*, is significantly increased in this region (at right of Figure 2.2). The first phase of saturated flow boiling region belongs to the bubbly flow regime. As $\overline{x}$, which denotes vapor mass fraction or vapor quality, increases, individual bubbles merge to create slugs of vapor. This is followed by the formation of an annular-flow regime in which a liquid film is created on the tube wall. The created film goes along the inner surface of the tube, while steam moves at a greater velocity through the center of the tube. Finally dry spots are formed on the inner surface of the tube and its size increases within a transition regime. Consequently, the tube surface will be entirely dry, and whole remaining liquid will be in the form of droplets that move at high velocity within the core of the tube in the mist regime. When all the droplets are vaporized, the second single–phase forced convection region consisting of superheated vapor is formed and the heat transfer coefficient is dramatically dropped. While the vapor fraction is increased along the tube length, along with a major difference in the densities of the liquid and vapor

phases, the mean velocity of the fluid will be increased drastically between the first and the second single phase forced convection regions (Incropera *et al*., 2006).

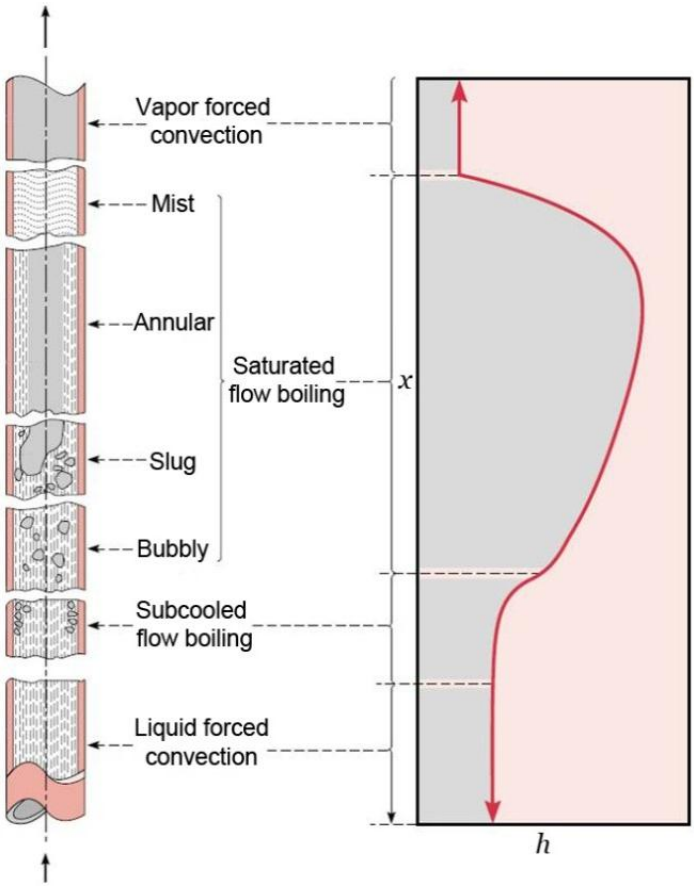

Figure 2.2 Flow regimes for forced convection boiling in a tube (Incropera, *et al.*, 2006)

2.3 Background

Figure 2.3 shows a qualitative flow boiling map of thermal behavior for flow boiling by Collier and Thome (1996). This study discusses the primary relationship between the vapor quality and heat transfer coefficient, with different heat flux values as a parameter. Vapor quality of the saturated two-phase region is represented with a positive value, while a negative value of vapor quality is represented to the subcooled region.

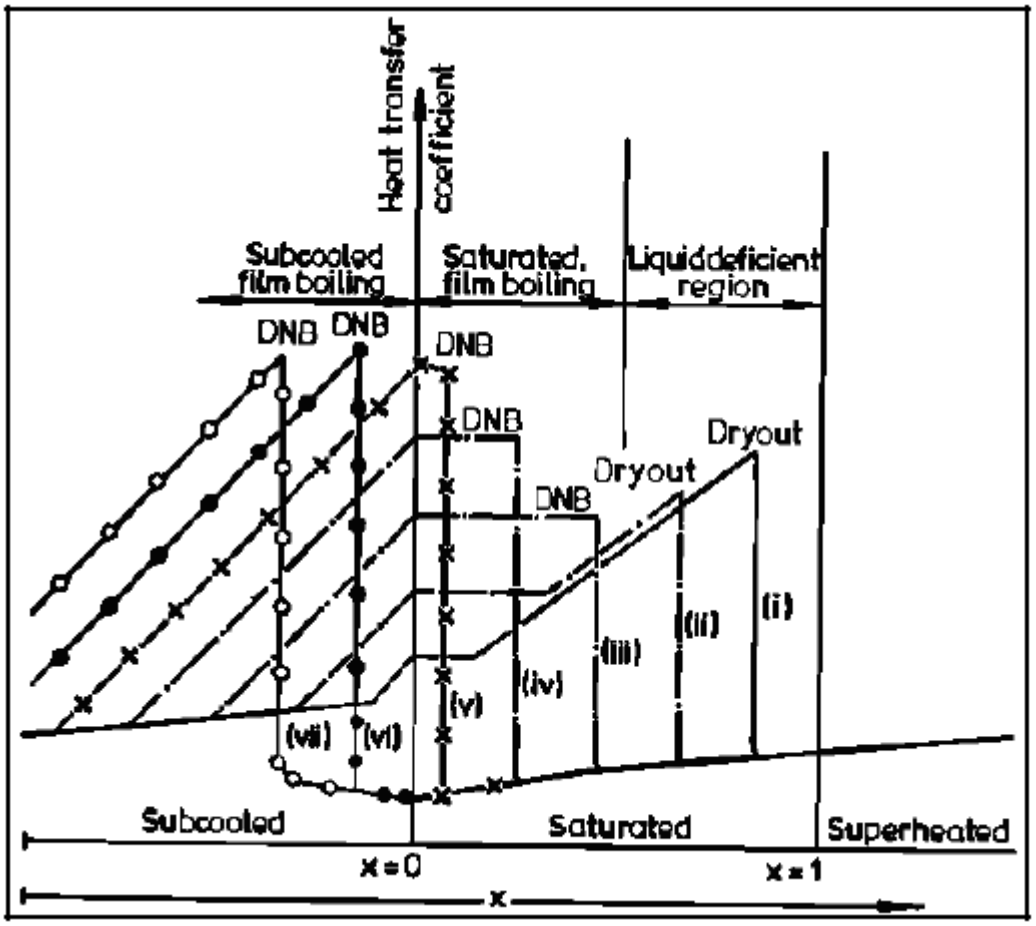

Figure 2.3 Schematic flow boiling map (Collier and Thome, 1996)

Each line in the map is presented with constant mass flux, *G*, and constant heat flux, *q*. In the single-phase liquid, the local convective heat transfer coefficient is constant because the influence of liquid temperature is not too great on the properties of the liquid. In the subcooled nucleate boiling region, the local heat transfer coefficient linearly increases because the difference between the wall and bulk liquid temperatures decreases linearly in along the tube length. The temperature difference between the wall and bulk liquid temperatures is constant in the saturated nucleate boiling region and thus the heat transfer coefficient remains constant. The heat transfer coefficient, *h*, increases when the heat flux rises from (i) to (vii). When the heat fluxes are at a low value, the liquid

deficient region is in the area of the dryout of annular film. Where the heat fluxes are the high value, the saturated film boiling is encountered to the process that moves from nucleate boiling *(DNB),* which this point is named by critical heat flux *(CHF).* The film boiling and an inverted annular flow can happen when vapor forms an annular film and there is liquid in the central core. In a condition of high heat flux, a decrease from nucleate boiling *(DNB)* may possibly occur in the subcooled region. This is becomes heat transfer coefficients in the wet wall region are greater than in the film boiling and liquid definition regions (Collier and Thome, 1996).

Kandlikar (1991a) built a flow boiling map to define the heat transfer coefficient as a function of major parameters such as vapor quality, heat flux, and mass flux. The map in Figure 2.4 shows the dimensionless parameters (i.e. two- phase flow boiling heat transfer coefficient over single-phase flow boiling heat transfer coefficient, h_{TP}/h_{lo}, and vapor quality *x*) that are developed. Vapor quality from negative value up to 0.8 is shown which covers the range from the onset of nucleate boiling in the subcooled region up to the saturated boiling region. In the subcooled flow region and saturated flow boiling region, the flow boiling map shows a progression using existing experimental and analytical evidence of the heat transfer mechanisms. These trends are achieved by correlations for the different regions. In circular tubes, effects on the heat transfer coefficient by most of the other important variable subcooled and saturated flow boiling regions are analyzed (Kandlikar, 1991). In the flow boiling map, the behavior of a variable that changes according to various circumstances during flow boiling is illustrated. The modified boiling number, *Bo*,* and density ratio, ρ_l/ρ_g, are used to calculate the two-phase flow boiling heat transfer coefficient over the single-phase flow

boiling heat transfer coefficient, h_{TP}/h_{lo}. ρ_l is the liquid density based on kg/m^3 and ρ_g denotes to vapor density based on kg/m^3. The modified boiling number, *Bo**, is introduced by Kandlikar (1991) and takes into account (1) the effect of the boiling number (*Bo*) that represents the effect of heat flux on nucleate boiling (Collier and Thome, 1996), and (2) the fluid-dependent parameter (F_{fl}). The saturated flow boiling region in Figure 2.4 consists of with two dominant regions such as the nucleate boiling and convective boiling dominant regions. The nucleate boiling dominant region happens at a lower value of vapor quality. The convective boiling dominant region exists at a higher value vapor quality. System parameters such as the density ratio, ρ_l/ρ_g, and *Bo** operations pressure, heat flux, and mass flux (*G*) are important in determining the variation of heat transfer coefficient along the nucleate boiling dominant and the convective boiling dominant regions. This flow-boiling map helps in the design and optimization of different flow boiling experiments, and also in interpreting the fundamental mechanisms (Kandlikar, 1991).

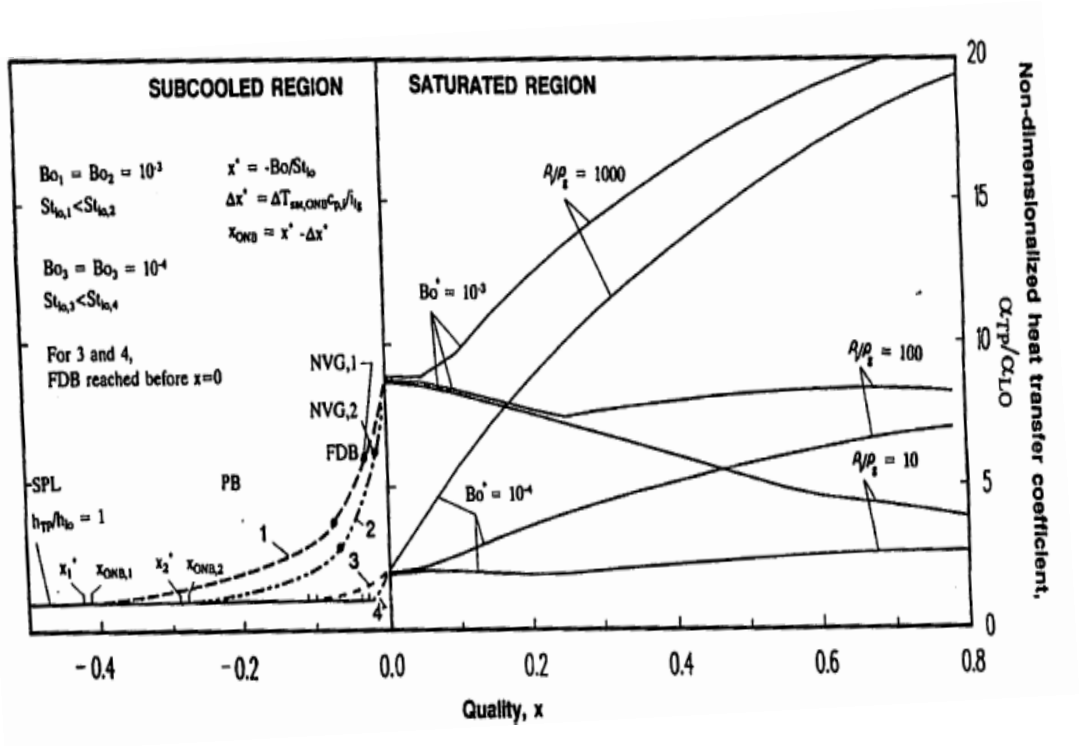

Figure 2.4 Initiated map for flow boiling regions in the vertical tubes with h_{TP}/h_{lo} versus xas coordinate by (Kandlikar, 1991a)

Other researcher of the flow boiling region has been done to gain a more fundamental understanding of the flow boiling phenomenon besides that for obtaining experimental studies (Kandlikar, 1990). A general empirical correlation is obtained for predicting saturated flow boiling heat transfer coefficients against vapor quality inside horizontal and vertical tube by (Kandlikar, 1990). The heat transfer coefficient, h_{TP}, along an evaporator tube with the proposed general correlation (Kandlikar, 1990) varies continuously against vapor quality, $\bar{x}$. The correlation is used for a number of fluids during flow boiling formation in plain circular tubes. The effects of various parameters and their correlations are investigated and analyzed. A general correlation for the condition of vertical flow liquid is developed for the two- phase flow boiling heat transfer coefficient, h_{TP}. The two-phase flow boiling heat transfer coefficient is the sum of

convective and the nucleate boiling terms. The effects of boiling number, convective number, constant heat flux and mass flux on the variation of heat transfer coefficient, h_{TP}, in these two terms are considered. The general correlation is extended to predict two-phase heat transfer coefficient to other fluids by using a fluid- dependent parameter, F_{fl}. The F_{fl} is a fluid–surface parameter that depends on the fluid and the heater surface characteristics. The introduction of F_{fl} is an important aspect of the Kandlikar correlation as the type of tube surface has a direct effect on the heat transfer coefficient. Table 1 gives values of the fluid-dependent parameters for several fluids in copper tubes (Kandlikar, 1990).

Table 2.1 Fluid parameter F_{fl} in the proposed correlation

Fluid	***F_{fl}***
Water	1.00
R-11	1.30
R-12	1.50
R-13B1	1.31
R-22	2.20
R-113	1.3
R-114	1.24
R-152a	1.10
Nitrogen	4.70
Neon	3.50
For stainless steel, F_{fl} =1 for all fluids	

In another research study (Saffari and Ghobadi, 2010) regarding the pressure drop along the vertical tube, the convective heat transfer coefficient and the wall temperature in a uniform heat flux for two-phase vertical flow are considered. The pressure drop effect on the flow and fluid properties for a two-phase flow boiling region at sub-atmospheric pressures cannot be ignored, because the pressure drop can be comparable to operating pressures. In this paper, the pressure drop, heat transfer, wall temperature, and properties of two-phase flow in a uniform heat flux on the onset nucleate boiling point at different sub-atmospheric conditions is analyzed. The total pressure drop increases along the tube because the initiation of bubbles causes a rise in the flow roughness (Saffari and Ghobadi, 2010).

Two conditions can be considered in order to calculate the heat transfer coefficient rate and energy rate of the flow in an enclosed tube. They are constant surface heat flux and constant surface temperature conditions. As shown in Figures 2.6, in a constant surface heat flux condition, the liquid mean temperature, T_m, varies linearly in the entrance and fully developed regions along the tube length. The heat transfer coefficient in entrance region is largely value due to the small difference between the surface temperature, T_s, and T_m but in the fully developed region, the heat transfer coefficient decreases due to the increasing difference between T_s and T_m (Incropera *et al.*, 2006).

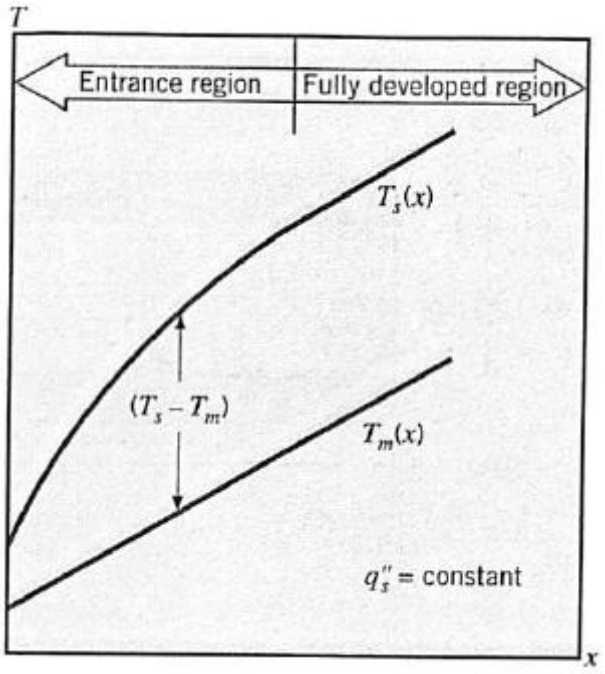

Figure 2.5 Temperature variations with constant surface heat flux condition in a tube

Figure 2.7 shows the plot for a constant surface temperature condition. The distribution of mean temperature for a liquid exponentially changes along the tube length. The temperature difference between surface and the liquid exponentially decays in distance along the tube length. The heat transfer coefficient increases exponentially (Incropera *et al*., 2006).

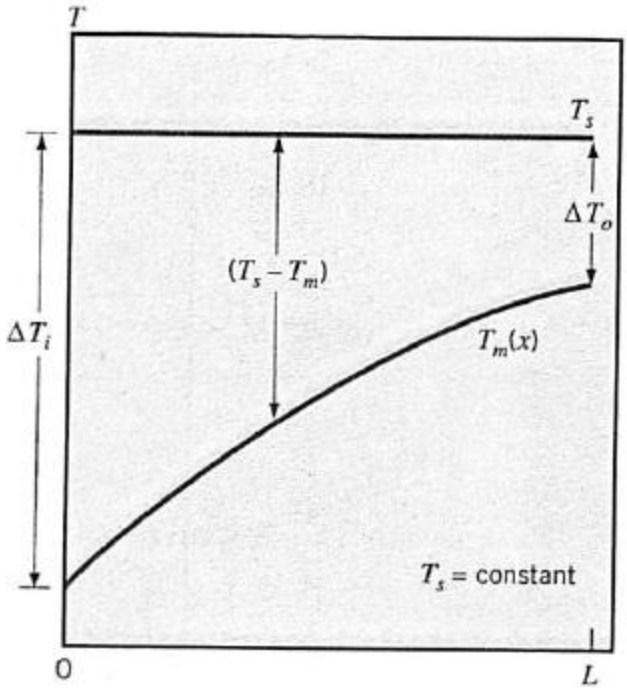

Figure 2.6 Temperature variation with constant surface temperature condition in a tube

In Ziadi *et al*. (2008), an experimental investigation of heat transfer of boiling distilled water under natural convective flow in a single pipe vertical thermosiphon reboiler is presented. The material used for the pipe is stainless steel. The test pipe is heated electrically. The variations in wall temperature are measured along its axis with thermocouples. In (Ziadi *et al*., 2008), the effect of heat flux and submergence, i.e. the fraction of heated tube volume which contains liquid water, on circulation rates is investigated. Also, the variation of local heat transfer coefficient along the heated pipe length for distilled water is considered. The results of this study show that the circulation rate for pure liquid depends mainly on heat flux, liquid submergence, inlet liquid sub-cooling and vapor fraction.

In Kamil *et al*. (1995), an experimental study of heat transfer for boiling liquids (e.g. distilled water, methanol, benzene, toluene, and ethylene glycol) has been carried out on

a single tube natural circulation reboiler. A stainless steel tube is used for test. The heat is transferred electrically to test a section of the tube with uniform heat flux. The effect of heat flux and liquid submergence on the variation of wall and liquid temperatures is discussed. The heat transfer coefficients in subcooled liquid and boiling region in the atmospheric pressure were calculated. The conclusion of this paper is that the heat flux and liquid submergence greatly influence the heat transfer coefficient and its variation along the tube (Kamil *et al*., 1995).

In Shamsuzzoha *et al.* (2004), an analysis of the onset of nucleate boiling for a vertical thermosiphon reboiler was investigated. The heat transfer coefficients at the onset of boiling are very high because of the nature of nucleate boiling and from a single-phase fluid to a two-phase flow. The point at which the two-phase region starts is called the incipient point of boiling, which corresponds to the condition of lowest amount of superheat or heat flux required for formation of the first vapor bubbles from the heated surface. The effect of submergence in natural circulation system was investigated. The result is that at constant submergence, as the heat flux increases, the superheated required for incipient boiling increases. At the low value of heat flux, the role of submergence has less effect than for high heat flux. Submergence is a significant parameter in the prediction of onset of nucleate boiling in a vertical thermosiphon reboiler (Shamsuzzoha *et al.*, 2004).

2.4 Summary

In chapter 2, different regions of water flow boiling in vertical tube are discussed and reviewed. Also, some previous research of subcooled, saturated, and vapor boiling regions are presented. Kandlikar correlations are used for different flow boiling regions

in the present study, which describes the flow boiling mechanism and analyzing flow boiling in the single vertical tube. Further discussion of Kandlikar correlations will be presented in the next chapter.

Chapter 3

3. Methodology

3.1 Introduction

To investigate the performance of a single vertical tube under various conditions, a simulation platform is developed. A dynamic model is considered for system optimization, which is formulated to analyze behavior of the thermodynamics and energy transfer processes in a single vertical tube in a solar collector. The model is designed (1) for different climates and/or latitudes with a constant wall surface temperature condition, and (2) for predicting the local heat transfer coefficient in different internal flow regions. The heat transfer coefficient at each location is estimated with the local pressure and constant surface wall temperature condition. The average daily solar irradiation in these territories and average surrounding temperature in warm and cold months during years reported in territories are used for the calculation of wall temperature. The energy equation is designed for evaluation of energy harvested.

According to the regions in Figure 2.2, different heat transfer mechanisms are dominant at different regions. Therefore, variations of heat transfer coefficients and theoretical mechanisms at different regions are expected. The heat transfer coefficient, h, is used in computing the heat transfer, which is typically by convection or phase change between a fluid and a solid. The local heat transfer coefficient h (W/m^2K) is based on the local wall temperature, the local bulk fluid temperature difference and the local heat flux, which represents the distribution of energy across the surface of an object, from the wall

into the fluid at the axial position along the tube assuming a uniform tube diameter (Kandlikar,1991). It is given as:

$$h = \frac{q}{(T_s - T_m)}, \tag{3.1}$$

where T_s (K) is the wall surface temperature, T_m (K) is the liquid mean temperature, and q (W/m^2) is the heat flux. The local heat transfer coefficients in different regions are presented in the following sections.

3.2 Subcooled Flow Region

In a vertical tube (refer to Figure 2.2) at a constant wall temperature condition, the water enters the tube below its boiling point and the heat on the tube surface is transferred to water. The first region, which is the subcooled flow region, is formed. In this region, the convection heat transfer mechanism is formed. The convective heat transfer coefficient h_{lo}(W/m^{2}K) in the subcooled liquid region can be considered in two flow conditions: laminar flow and turbulent flow (Incropera, *et al*., 2006).

Laminar flow is a motion of the particles of fluid that is arranged with all particles moving in straight lines parallel to the tube walls (Incropera, *et al*., 2006). Reynolds number, Re_D, is a nondimensional number that helps to determinate laminar or turbulent flow. Reynolds number Re_D provides a quantity of the ratio of inertial forces to viscous forces and measures the relation of these two forces for given flow circumstances (Incropera, *et al*., 2006). When The Reynolds number value is less than 2300, the liquid flow is assumed to be a laminar flow. Re_D is given as (Incropera, *et al*., 2006):

$$Re_D = \frac{4\dot{m}}{D\pi\mu_l}, \tag{3.2}$$

where ρ_l, μ_l, $\dot{m}$ and D are the density of liquid (kg/m^3), the viscosity of liquid (Ns/m^2), mass flow rate (kg/s), and tube inner diameter (m), respectively.

The local convection heat transfer coefficient, h_{lo}, can be written as follows (Incropera, *et al*., 2006):

$$h_{lo} = \frac{Nu_D \times k_l}{D} \qquad Re_D < 2300 \tag{3.3}$$

where Nu_D is Nusselt number and k_l (W/mK) is the local thermal conductivity of the liquid. The local thermal conductivity is a function of local liquid temperature.

For heat transfer on a surface in a fluid, The Nusselt number is a nondimensional number that represents the ratio of convective to conductive heat transfers across the surface. At a uniform surface wall temperature, T_s (K), Nu_D is a constant dimensionless number with a value of 3.66 (Incropera, *et al*., 2006).

Turbulent flow condition is the irregular nonlinear flow of a fluid caused by high velocity (Incropera, *et al*. 2006). The local subcooled heat transfer coefficient, h_{lo}, with a turbulent flow condition can be calculated by empirical correlations based on the Prandtl number, *Pr*, of different fluids, Reynolds number and fraction factor at two conditions given (Kandlikar, 1991):

1. $(0.5 \leq Pr \leq 2000 \text{ and } 2300 \leq Re_D \leq 10^4)$,

$$Nu_D = h_{lo}\frac{D}{k_l} = \frac{(Re_D - 1000)(f/8)Pr}{1+12.7(f/8)^{1/2}(Pr^{2/3}-1)} \ . \tag{3.4}$$

2. $(0.5 \leq Pr \leq 2000 \text{ and } 10^4 \leq Re_D \leq 5 \times 10^6)$,

$$Nu_D = h_{lo}\frac{D}{k_l} = \frac{Re_D(f/2)Pr}{1.07+12.7(f/2)^{1/2}(Pr^{2/3}-1)} . \tag{3.5}$$

The Prandtl number Pr is a nondimensional number. The ratio of momentum diffusivity (kinematic viscosity) to thermal diffusivity as the equation given:

$$Pr = (\nu/\alpha)\,, \tag{3.6}$$

where ν, α and f are momentum diffusivity, thermal diffusivity (m^2/s) and the single-phase liquid friction factor, respectively.

The friction factor f for the two correlations above is defined as:

$$f = [1.58\ln(Re_D) - 3.28]^{-2}\,. \tag{3.7}$$

The fraction factor is a dimensionless number and determined by pressure drop. Equipment, such as a pump, is used for overcoming the pressure drop in a tube.

While the heat is transferred from the wall's constant surface temperature to the liquid flow, the liquid outlet mean temperature, $T_{m(z)}$, along the tube subcooled flow region increases exponentially. The liquid mean temperature profile along tube subcooled flow region can be calculated by (Incropera *et al*., *2006*):

$$\frac{T_s - T_{m(z)}}{T_s - T_{m,i}} = \exp\left(-\frac{D.\pi.z.\overline{h_{lo}}}{\dot{m}.c_{p,f}}\right) \tag{3.8}$$

where $T_{m(z)}$, $T_{m,i}$, T_s, $c_{p,f}$, $\dot{m}$, z, D and $\overline{h_{lo}}$ are liquid outlet mean temperature in axial position z, liquid inlet mean temperature (K) wall temperature (K), specific heat (kJ/kgK), mass flow rate (kg/s), axial position within the tube length, L (m), tube diameter (m) and average convection heat transfer coefficient (W/m^2K) in subcooled flow region, respectively.

The average convective heat transfer coefficient, $\overline{h_{lo}}$, along tube subcooled flow region according to the liquid average thermal conductivity, $\overline{k_l}$, that is function of liquid temperature as:

$$\overline{h_{lo}} = \frac{Nu_D \times \overline{k_l}}{D}. \quad (3.9)$$

The average thermal conductivity is determined by the average of liquid thermal conductivity at inlet temperature and thermal conductivity at saturation temperature.

When heat is transferred from wall to liquid in upward flow, a change of phase and difference in density occurs. The change of phase and density, and the increase of vapor quality along tube length increase the velocity of the fluid. According to the initial values of parameters such as the liquid inlet temperature, liquid saturation temperature, the tube length between inlet and saturation temperature, wall temperature and the average heat transfer coefficient calculated based on average thermal conductivity at the subcooled flow region, the mass flow rate can be obtained by Equation (3.8).

3.3 Saturated Flow Boiling Region

The saturated boiling flow region starts from a point where the thermodynamic vapor quality reaches zero and water boils at saturation temperature. The saturation temperature is the temperature for a corresponding saturation pressure at which water boils into its vapor phase. The saturation temperature, T_{sat} , along the saturated boiling flow region is constant. The vapor quality in this region increase until a vapor quality of 1 is reached. After reaching a vapor quality of 1, the phase of fluid reaches another region called vapor region.

In the saturated flow boiling region, the heat transfer mechanism is divided into (1) the convective boiling dominant (CBD) region (2) the nucleate boiling dominant (NBD) region (Kandlikar *et al*., 1999). The convective and nucleate boiling heat transfer contributions are formulated directly from empirical relationships, which can be

calculated by the two-phase heat transfer coefficient, h_{TP}, with a constant heat flux condition along the saturated flow boiling region. The heat transfer coefficient of the nucleate boiling dominant region (NBD) is given as:

$$(h_{TP})_{NBD} = \underbrace{h_{lo}(0.6683(\rho_l/\rho_g)^{0.1}\bar{x}^{\,0.16}(1-\bar{x})^{0.64}f_2(Fr_l))}_{\text{Convective boiling term}} + \underbrace{h_{lo}(1058Bo^{0.7}F_{fl}(1-\bar{x})^{0.8}).}_{\text{Nucleate boiling term}} \quad (3.10)$$

The heat transfer coefficient of the convective boiling dominant region (CBD) is written as:

$$(h_{TP})_{CBD} = \underbrace{h_{lo}(1.136(\rho_l/\rho_g)^{0.45}\bar{x}^{\,0.72}(1-\bar{x})^{0.08}f_2(Fr_l))}_{\text{Convective boiling term}} + \underbrace{h_{lo}(667.2Bo^{0.7}F_{fl}(1-\bar{x})^{0.8}).}_{\text{Nucleate boiling term}} \quad (3.11)$$

The maximum value of the heat transfer coefficient, h_{TP}, calculated in Equations (3.10) and (3.11) should be used (Kandlikar, 1991), that is $h_{TP} = \max\left[(h_{TP})_{NBD},(h_{TP})_{CBD}\right]$. ρ_l, ρ_g, $\bar{x}$, ρ_l/ρ_g, Bo, F_{fl} and $f_2(Fr_l)$, are liquid density (kg/m^3), vapor density (kg/m^3), vapor quality, density ratio, boiling number, fluid-dependent parameter and the stratification parameter, respectivily. F_{fl} is a fluid-dependent parameter, which is 1.0 for water. $f_2(Fr_l)$ is the stratification parameter which accounts for stratification of liquid and vapor phases in horizontal or vertical tubes; 1.0 for a vertical tube. All properties of two-phase flow boiling correlations must be calculated using the saturated boiling temperature.

The correlations in Equations 3.10 and 3.11 are valid for the mean vapor mass fraction ranging $0 \leq \bar{x} \leq 0.8$. The local mean vapor mass fraction or vapor quality, $\bar{x}$, at saturated flow boiling region can be found:

$$\bar{x}_{(x)} = \frac{q.\pi.D.x}{\dot{m}.h_{fg}} \quad (3.12)$$

Bo is equal to boiling number and is defined as:

$$Bo = \frac{q}{Gh_{fg}} \tag{3.13}$$

where h_{fg} and G are heat of vaporization (kJ/kg) and mass flux (kg/m^{2}s). The boiling number is a dimensionless number involving the heat flux over mass flow rates per unit area and the heat of vaporization or effect of heat flux on nucleate boiling (Collier and Thome, 1996).

Mass flux, *G*, is defined as mass flow rate per unit cross-sectional area (m^2) of the tube. The mass flux along the tube length is constant because mass flow rate along inside tube length and sectional area of tube are constants (Saffari and Ghobadi, 2010). The mass flux can be found as (Incropera *et al*. 2006):

$$G = \frac{\dot{m}}{A} \tag{3.14}$$

Remember that Equations (3.10) and (3.11) are for the cases of constant heat flux. For a constant wall temperature circumstance, heat flux, *q*, varies along saturated flow boiling region (Incropera *et al*. 2006). Therefore, an iteration method, called secant method (Kincaid, 2002), is used to find the appropriate heat flux, *q*, and two-phase heat transfer coefficient for each segment in the saturated flow boiling region. The vertical tube has been divided into a number of segments that is 200 in the present study. Each segment is assumed to have constant heat flux. This number of segments was selected in consideration of having a computational efficiency with minimum error. At the first step, $q_{(0)}$ is the maximum value of heat flux in subcooled flow region and $q_{(1)}$ is $q_{(0)}$*2. Two initial values of heat flux, $q_{(0)}$ and $q_{(1)}$, are presented in Equation (3.15). The initial Error, $E_{(1)}$, is considered 1 and Error threshold, E_t, is defined as equal to 0.001W/m^2 which is far below the minimum heat flux (around 4W/m^2) calculated in the following chapters.

The maximum error involved is less than 0.025%. The maximum of $(h_{TP})_{NBD}$ and $(h_{TP})_{CBD}$, will be calculated from Equations (3.10) and (3.11), respectively, with the estimated q. From general Equation (3.1), Equation (3.16) is presented for saturated flow boiling region. When the final h_{TP} value is extracted from (3.10) and (3.11), it will be placed in Equation (3.16) and a q can be estimated. Then the values of $q_{(0)}$ and $q_{(1)}$, which are initialized before, will be subtracted from generated q in equation (3.15). The difference between $q_{(0)}$ and q as well as $q_{(1)}$ and q are considered as new estimated errors, $E_{(0)}$ and $E_{(1)}$ respectively (Kincaid *et al*. 2002).

$$q_{(n+1)} = q_{(n)} - E_{(n)}\left[\frac{q_{(n)}-q_{(n+1)}}{E_{(n)}-E_{(n-1)}}\right] \qquad (n \geq 1) \tag{3.15}$$

$$h_{TP}(T_s - T_{sat}) = q \tag{3.16}$$

After computing these results, the error numbers and q values will be set in equation of (3.15) which is the secant iteration method. This will produce a new $q_{(n+1)}$ that will be available for a new iteration. The iterations will continue until the produced error become smaller than threshold error, which is 0.001. When the error is less than the threshold error then the iteration will stop and $q_{(n+1)}$ will be considered as the resultant local heat flux. Recalling this iteration method will be computed for each local point in the saturated flow boiling region.

3.4 Vapor Region

After the droplets have vaporized in the saturated flow boiling region, the fluid reaches to a second single-phase forced convection region. The properties of the fluid are based on the vapor in this region. The heat transfer coefficient in this region is the convection mode. The equations for finding temperature profile and heat transfer

coefficient at the vapor forced convection region are the same as the subcooled flow region except that the properties are based on vapor characteristics. For example, below is the equation of Nusselt number.

$$h_g = \frac{Nu_D \times k_g}{D} \tag{3.17}$$

Where h_g and k_g are single-phase vapor heat transfer coefficient (W/m^{2}K) and vapor thermal conductivity (W/mK).

All the liquid and vapor properties in subcooled flow, saturated flow boiling and vapor regions are determined using the liquid and vapor temperature. Properties' values can be found at The International Association for the Properties of Water and Steam Website (IAPWS, 2007).

3.5 Total Heat Transfer Rate

Heat transfer rate is the energy transfer due to temperature differences in an element. The rate of heat transfer in a certain direction depends on the amount of the temperature rise along that direction. The increase of the rate of heat transfers occurs as the temperature gradient between two points increases (Incropera *et al*. 2006).

A fluid of velocity u and mean temperature T_m flows over a surface of the circular tube with area A_s. While the tube surface is at a uniform wall temperature condition, the natural convection heat transfer in the subcooled flow is caused by buoyancy forces due to the temperature differences and thus the density changes in the fluid. The natural convection heat transfer is a transfer of fluid sensible energy. At later stage of the process, the latent heat exchange is generally associated with a phase change between the liquid and vapor states of a fluid, which is related to the process of boiling and

condensation in the flow boiling region. Finally, the states of fluid are completely changed to single-phase vapor. Both the local heat transfer coefficient and local surface heat flux vary along the tube length. The total heat transfer rate $\dot{Q}(W)$ along the tube length is obtained by integral of the local heat flux over the entire surface as (Incropera *et al*. 2006),

$$\dot{Q}_{total} = D.\pi \int_0^L q_{(z)} dz \qquad (3.18)$$

where D, L and $q_{(z)}$ are tube inner diameter, tube length, heat flux, respectively.

3.6 Uniform Tube Surface Temperature

An equation is needed to model tube surface temperature regarding the amount of average daily solar radiation and surrounding temperature of each territory of a country. For determination of tube surface temperature, two parameters are required. They are solar radiation and surrounding temperature. Both of which are presented as follows.

3.6.1 Solar Radiation

The solar flux is the distribution of sun's energy arriving at the Earth's atmosphere. The solar radiation is portion of this solar flux, which is 99.97% (WIK, 2012). Solar radiation is the energy given off by the sun in all directions. The amount of solar radiation is powerfully reliant on atmospheric conditions, the time of year, and the angle of incidence. The solar radiation incident on the earth's surface is dependent on the atmospheric content of dust and other contaminants; hence all the energy expressed by the sun does not reach the surface of earth. A large amount of solar energy spreads out over the surface of the earth when the rays have a straight incident on the surface. Also, if the solar rays travel a smaller distance with a zero angle from normal, more energy will

be reached to the surface compared to rays that a greater angle from normal(Holman, 1992). The solar radiation energy can be considered in term of insolation, which is the solar irradiation received over a period of time, typically one day. It is typically expressed as kWh/m^2/day. The solar irradiation is the total amount of solar energy accumulated on an area over time. Insolation is usually used to rate the solar energy potential of a location by calculation of the average energy received on a surface per day (PV, 2010). From the radiation equilibrium equation, the equilibrium temperature for black lacquer tube surface, T_S, given as follows (Holman, 1992):

$$\left(\frac{q}{A}\right)_{sun} \alpha_{sun} = \alpha_{low\ temp}\sigma\left({T_s}^4 - {T_{surr}}^4\right) \qquad (3.19)$$

where $\left(\frac{q}{A}\right)_{sun}$, α_{sun}, $\alpha_{low\ temp}$, σ, T_{surr}, T_s are solar flux, (W/m^2), absorptivity for solar radiation, absorptivity for low-temperature radiation, Estefan-Boltzmann constant (W/m^{2}K^4), surrounding temperature (K) and wall temperature (K), respectively. Table 3.1 shows the solar radiation absorptivity of different objects in low-temperature. Absorptivity for solar radiation, α_{sun}, and absorptivity for low-temperature radiation, $\alpha_{low\ temp}$, on black lacquer surface is 0.96 and 0.95, respectively (Holman, 1992). The amount of Estefan-Boltzmann constant, σ, is 5.669×10^{-8}(W/m^{2}K^4), As shown in Table 3.1, the solar radiation absorptivity of opaque objects in low-temperatures is more than a for clear objects (Holman, 1992).

Table 3.1 Comparisons of Absorptivity of a Variety of Surfaces to Solar and Low-Temperature Thermal Radiation

Surface	***Absorptivity***	
	For solar radiation	***For low-temperature radiation ~ 25 C***
Aluminum, highly polished	0.15	0.04
Copper, highly polished	0.18	0.03
Tarnished	0.65	0.75
Cast iron	0.94	0.21
Stainless, no. 301, polished	0.37	0.60
White marble	0.46	0.95
Asphalt	0.90	0.90
Brick, red	0.75	0.93
Gravel	0.29	0.85
Flat black lacquer	0.96	0.95
White paints, various types of pigments	0.12-0.16	0.90-0.95

Figure 3.2 (NREL, 2008) presents the amount of solar irradiation ($Wh/m^2/day$) in the territories of the United States. The solar irradiation values in the map are established from the National Solar Radiation Data Base (NSRDB). The average values of solar irradiation for different regions are displayed in the map. The points shown on the map are different areas in the U.S. The average solar irradiation values are completed by

averaging all 30 years of data for each area. With regard to the present solar irradiation in each territory, the amount of solar flux $\left(\frac{q}{A}\right)_{sun}$, can be calculated (NREL, 2008).

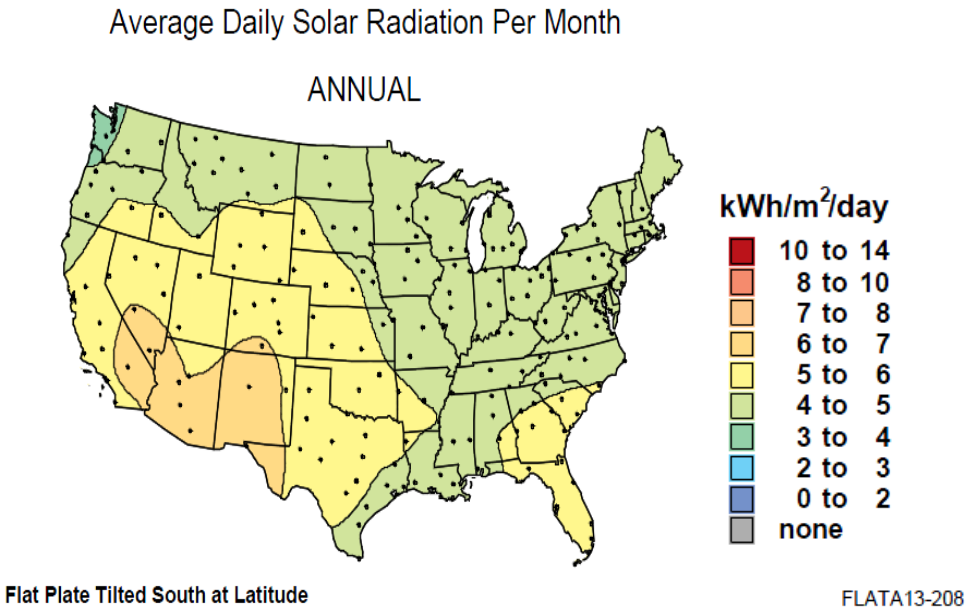

Figure 3.1 Map of solar irradiation distribution, (NREL, 2008)

3.6.2 Surrounding Temperature

The surrounding temperature, T_{surr}, for each territory of a country can be calculated from the average temperature of warm and cold months during the years reported (for instance, Weather Channel, Omaha). The average temperature of Omaha, Nebraska is chosen for this system design. The maximum and minimum temperature of each month for Omaha is shown in Figure 3.3. January, February, November and December, have lowest temperatures during the average year in Omaha (TWC, 2012). The surrounding temperature for this system design is selected from the average temperature of the coldest months. The reason for choosing the lowest temperature is to design a system that will eliminate freezing at the coldest month of year.

Figure 3.2 Graph of monthly average temperatures of Omaha (TWC, 2012)

3.7 Summary

In this chapter, the correlations and their formulations for calculating heat transfer coefficients, total heat transfer rate, and fluid temperature at different flow-boiling regions and conditions are discussed. Calculation of wall surface temperature is formulated based on solar radiation and ambient temperature. Also a map is presented

with values of solar radiation for each area of the U.S to be used in calculating solar flux. The results and discussion of this research is represented in the next chapter.

Chapter 4

4. Analysis and Optimization

4.1 Introduction

As stated earlier in chapter 1, the main purpose of the current study is to analyze and optimize the performance efficiency of a single tube in a domestic hot water system based on a boiling-condensing cycle. In order to achieve this task, it is necessary to know how to maximize the heat transfer coefficient and the total heat transfer rate in the solar collector tube. Equations and empirical correlations introduced in Chapter 3 will be used to model the processes of a boiling-condensing cycle and to understand thermal behavior and energy transfer processes in vertical single tube.

The investigation of the heat transfer coefficient and system performance is based on a parametrical analysis of design parameters (for instance, various pressures with fixed tube size) in a dynamic model. Subatmospheric pressures are adopted inside the tube because it will present the solar domestic water heating systems not freezing in the climates where very low temperatures occur.

A computer simulation program is written with MATLAB and developed based on the dynamic model for better understanding and analyzing of solar thermodynamic behavior. The objective of this program is to estimate the heat transfer coefficient, heat flux, and total heat transfer rate which are the functions of parameters including vapor quality, wall temperature, mass flow rate, tube diameter, tube length and pressure inside the tube. The changes of the surface heat flux and fluid temperature profile are simulated in different flow regions. The thermodynamic processes for subcooled flow region,

saturated flow boiling region and single-phase vapor region (superheat region) are simulated.

In this analysis section, plots of water temperature profile and heat flux along the tube are presented. Heat transfer coefficients in different regions are sketched based on a tube diameter and internal pressures. Separately in each region, different properties (such as, various pressure characteristics, fluid density, thermal conductivity, and etc.) are presented to analyze the heat transfer coefficient, surface heat flux and total heat transfer rate. Properties for subcooled and vapor regions are calculated from a method called XSteam in MATLAB software, which has IAPWS (2007) as its reference. The properties of saturation region are shown in Table 4.1 (Incropera *et al*., 2006).

4.2 Process parameters

In the present study, distilled water is the working fluid inside the black lacquer copper tube. A tube diameter of 0.03 meter is used. The length of the solar collector tube is 2 meters long. The inlet water temperature into the tube is set to be 5 degree Celsius less than the saturation temperature of the specific pressure to ensure that pure liquid entering the inlet. The tube inlet temperature is controlled by valve installed where the heated water passes from the heat exchanger. Subatmospheric pressure is used for this study. Properties of saturated water in the tube are represented in Table 4.1 (Incropera *et al*., 2006). There are four different pressures presented in this study.

Table 4.1 Thermophysical properties of saturated water

Pressure ***Properties***	P1	P2	P3	P4
Saturation pressure (Pa)	3531	2617	1917	1387
Saturation temperature (K)	300	295	290	285
Liquid specific volume (m^3/kg)	0.001003	0.001002	0.00100	0.001
Liquid specific density (kg/ m^3)	997	998	999	1000
Vapor specific volume (m^3/kg)	39.13	51.94	69.7	99.4
Vapor specific density (kg/ m^3)	0.0255	0.019	0.014	0.010
Latent heat of vaporization (J/kg)	2438000	2449000	246100	247300
Liquid specific heat (J/kg.K)	4179	4181	4184	4189
Vapor specific heat (J/kg.K)	1872	1868	1864	1861
Liquid viscosity (N.s/m^2)	0.00085	0.000959	0.00108	0.00122
Vapor viscosity (N.s/m^2)	0.000009	0.0000088	0.0000086	0.0000084
Liquid thermal conductivity (W/m.K)	0.613	0.606	0.598	0.590
Vapor thermal conductivity(W/m.K)	0.0196	0.0195	0.0193	0.0189
Liquid Prandtl number	5.83	6.62	0.0756	8.81
Vapor Prandtl number	0.857	0.849	0.841	0.833

Solar flux is assumed to be 190 W/m^2, which is the average value for Omaha, Nebraska. According to Equation (3.19), the temperature of the tube wall is calculated

based on solar flux an average of the lowest temperature for the coldest months in Omaha, e.g. -8 ^{o}C. The wall temperature is considered to be 302.6 K.

4.3 Research analysis

In this section, single-phase and two-phase flow development in a vertical tube were simulated and analyzed to gain a better understanding thermodynamic behavior of fluid flow in phase different regions and different pressures. The single tube configurations of heat transfer process are shown in Table 4.2.

Table 4.2 Parameters of a test

T_s (K)	D (m)	P (Pa)	L (m)	Z_f (m)	T_{sat} (K)	T_i (K)
302.6	0.03	3531	2	0.5	300	295

For the case of saturation pressure, P, at 3,531Pa (i.e. Case P1 in Table 4.1), the water inlet temperature, T_i, is 295K. The saturation water temperature, T_{sat}, is 300K. The length of subcooled flow region, Z_f that is the length from tube inlet to the point at saturation water temperature, is 0.5m. Z_f and T_i are used to determinate mass flow rate and average heat transfer coefficient in subcooled flow region. The estimated mass flow rate, $\dot{m}$, is 0.0006745kg/s from Equation 3.8, which is a constant throughout all regions, consisting of the subcooled flow, saturated flow boiling and vapor regions. The Reynolds number is 33.13 and less than 2300; therefore, the liquid flow is laminar.

4.3.1 Analysis of water temperature profile

For constant wall temperature, the liquid temperature profile along the tube (2m in length) is shown as Figure 4.1. Horizontal axis represents the coordinate, z [m], along the

2-meter-length pipe from water inlet, while vertical axis is the liquid and wall temperatures, respectively. The red line shows the constant wall temperature along the tube due to solar irradiation. The black line is liquid temperature in different flow boiling region.

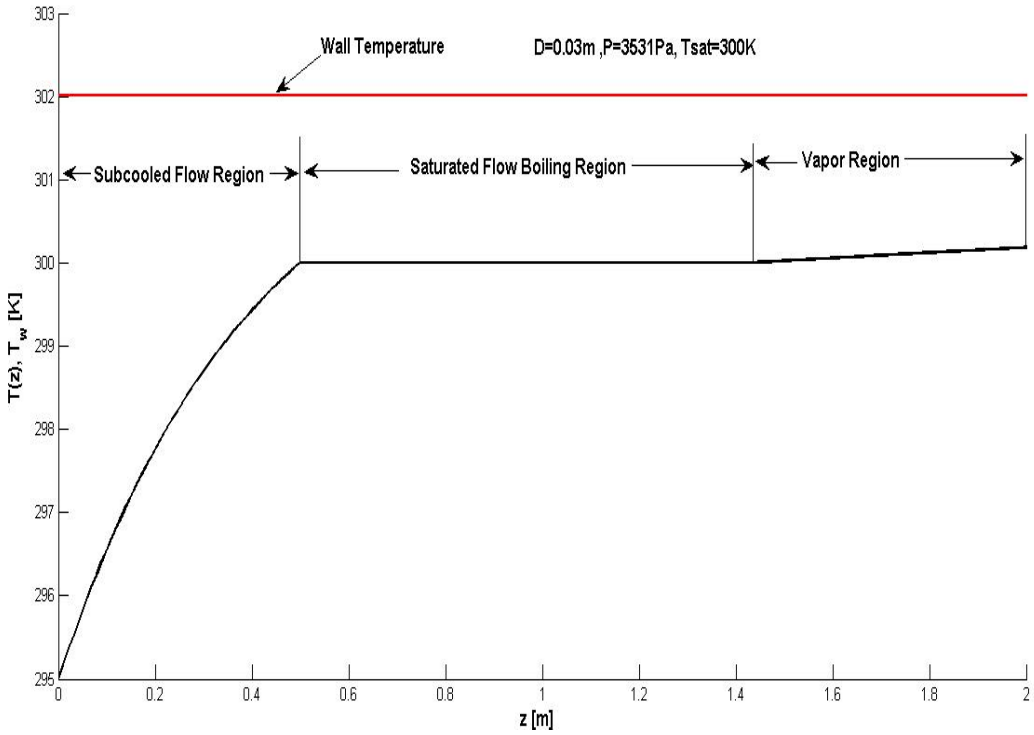

Figure 4.1 Water temperature profile; Pressure 3531Pa; Tube diameter 0.03m

In the subcooled flow region, the water temperature increases exponentially from 295 K to 300K as *z* increases, due to convective heat transfer. The temperature difference between the wall temperature and the water temperature reduces as *z* increases. After reaching the saturation water temperature at 300K, the water boils and the temperature is constant in the saturation region (at saturation temperature) until it reaches its fully vapor phase at saturation pressure. After the saturated flow boiling region, the vapor

temperature in the vapor region increases gradually due to convective heat transfer along the tube based on Equation 3.8. The temperature difference between wall temperature and vapor temperature reduces as *z* increases.

4.3.2 Analysis of heat transfer coefficient in subcooled flow region

Figure 4.2 presents a plot of the heat transfer coefficient, *h*, along the tube, *z*, at a pressure of 3531Pa and a tube diameter of 0.03m. Three different regions of flow boiling are shown. The first section of the graph which is from the entrance of the tube to the beginning of saturated flow boiling region is called subcooled flow region. To better show that the subcooled flow region plot, the heat transfer coefficient along x-axis, *z* is zoomed in Figure 4.3.

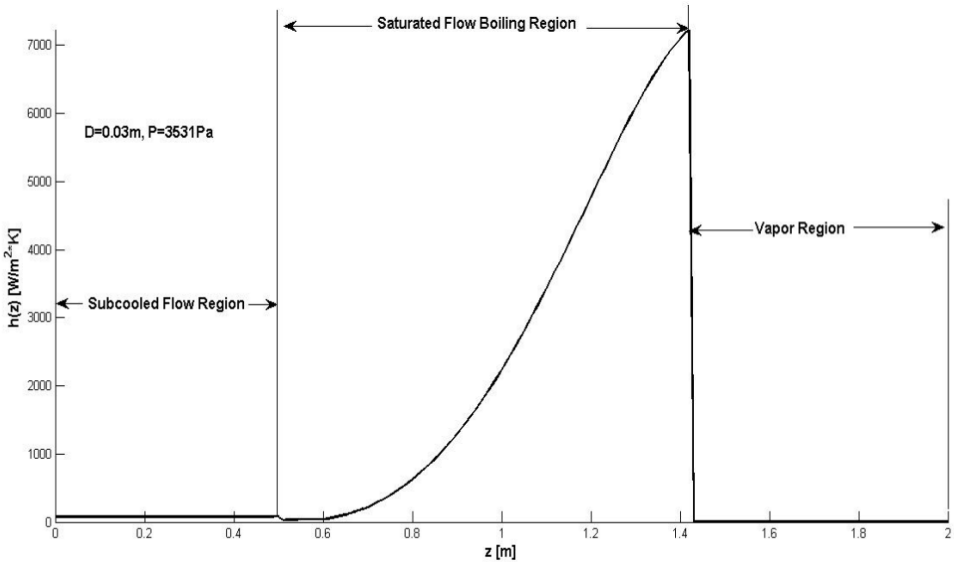

Figure 4.2 Heat transfer coefficient in different regions along a 2-m tube; Pressure 3531 Pa; Tube diameter 0.03m

As presented in Figure 4.3, the heat transfer coefficient increases gradually along z because the thermal conductivity of water is increasing due to the heat transfer of wall

temperature to water and sensible heat in the subcooled flow region. The sensible heat is exchanged and thus the temperature increases.

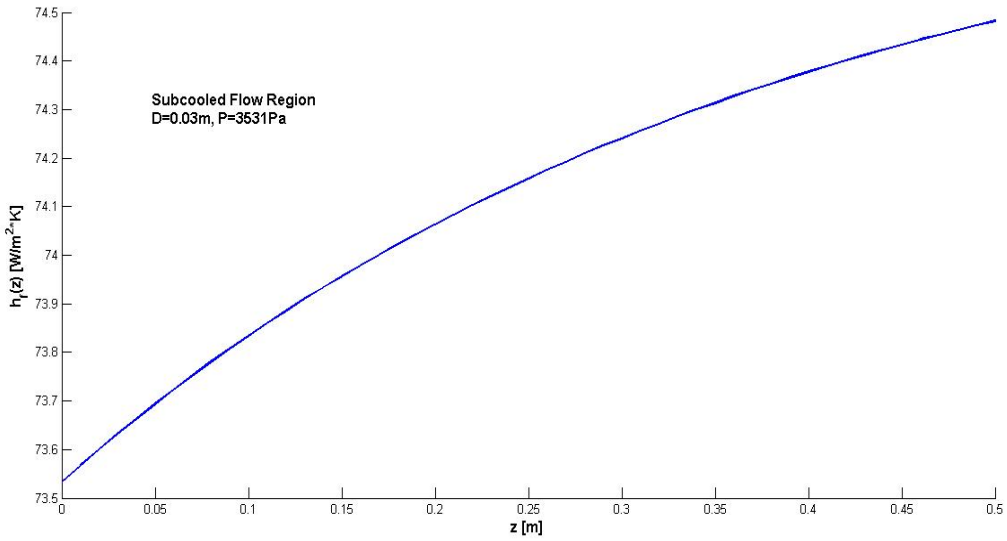

Figure 4.3 Heat transfer coefficient at subcooled flow region along tube; Pressure 3531 Pa; Tube diameter 0.03m

4.3.3 Analysis of heat transfer coefficient in saturated flow boiling region

In Figure 4.2, the heat transfer in the two-phase saturated flow boiling region consists of convective and boiling modes. The heat transfer coefficient dramatically increases along *z*. In this region, the thermodynamic quality (vapor quality) is between 0 and 1. The range of vapor quality, $\bar{x}$, in the saturated flow boiling region is in a range of $0 \leq \bar{x} \leq 0.8$ in the present study due to the limitations of Kandlikar correlation. In consideration of limited contribution of the section with $0.8 < \bar{x} \leq 1$ in total heat transfer rate, this small section is ignored in the present study without significant error on total heat transfer rate. Because of this reason, the heat transfer coefficient in the saturation region drops suddenly in the beginning of vapor region.

The saturation flow boiling region is divided into two dominant regions which are the nucleate boiling dominant region (*NBD)* and the convective boiling dominant (*CBD*) region. As Figure 4.2 shows, at the end of subcooled flow region there is a small downward slope and then an increasing trend in the saturation flow boiling region. Figure 4.4 shows the same graph of Figure 4.2 but zooms in to the end of the subcooled flow region and the beginning of saturation region. This small downward slope is relevant to the nucleate boiling dominant (*NBD*) region (see Figure 4.4). The nucleate boiling dominant region occurs at the low vapor quality in the beginning of the saturated flow boiling region (see rectangle in Figure 4.4).

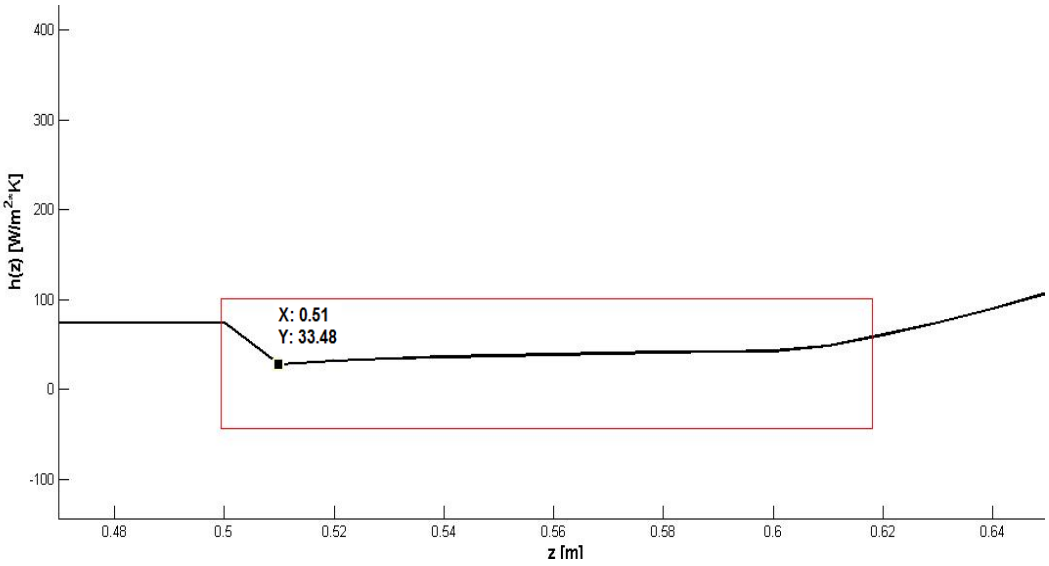

Figure 4.4 Heat transfer coefficient in the transition between subcooled, nucleate boiling dominant, and convective boiling regions against *z*; Pressure 3531 Pa; Tube diameter 0.03m

As shown in Figure 4.4, the heat transfer coefficient in the nucleate boiling dominant region, i.e. the small downward trend, decreases initially since the nucleate boiling component, water, is reducing because of increasing vapor quality (see Figure 2.1 in area between *NVG* and *H*). Therefore, the amount of water plays the main role in convective

heat transfer coefficient increase. In Figure 4.4, following the decreasing slope of nucleate boiling dominant region, there is a plateau in the beginning of the convective boiling dominant region because the effect of nucleate boiling still exists.

After the plateau in the start point of convective boiling dominant region, around point 0.52m in the tube length, the dramatic upward trend curve is observed in the saturated flow boiling region (see Figure 4.2). It indicates convective boiling dominate region. This region occurs where mass fraction of vapor increases. In the convective boiling dominant region, the two-phase heat transfer coefficient is greatly influenced by vapor quality, $\bar{x}$. The amount of vapor is significantly high in this region. Increase of vapor quality, $\bar{x}$, and significant difference in the densities of water and vapor cause the velocity of fluid and the heat transfer coefficient to increase. After the saturation region, flow reaches to the vapor region.

4.3.4 Analysis of heat transfer coefficient in vapor region

In the vapor region, there are no water droplets because the water is completely vaporized. In Figure 4.2, the vapor region starts with a vapor quality of 0.8 after the saturation region in the present study. The heat transfer mode in this region is convective and the heat transfer coefficient significantly decreases after the saturation region. The reason for the drop in the heat transfer coefficient is that thermal conductivity of vapor is small compared with other regions. In the vapor region, with additional heat to the vapor and the effect of sensible heat transfer, the thermal conductivity of vapor increases based on the increase of vapor temperature (See Figure 4.1) along the vapor region. Therefore the convective heat transfer coefficient slightly increases based on Equation (3.17). To better present the increase in heat transfer coefficient in the vapor region, the heat transfer

coefficient along *z* is zoomed in Figure 4.5. As presented in Figure 4.5, the increase of heat transfer coefficients is very small and it changes from 2.254W/m^{2}K to 2.256W/m^{2}K in the vapor region.

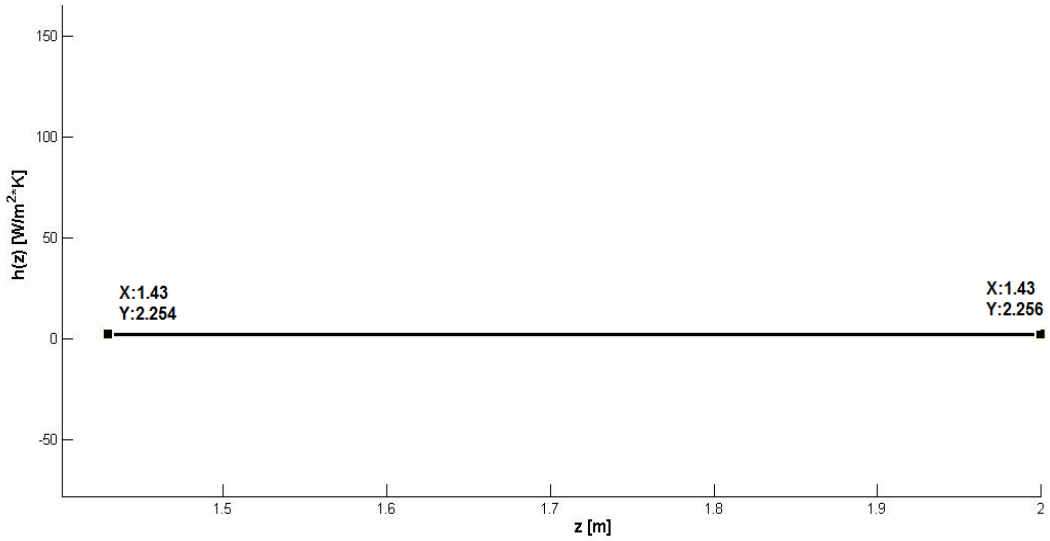

Figure 4.5 Heat transfer coefficient in vapor region against *z*; Pressure 3531Pa; Tube diameter 0.03m

4.3.5 Analysis of heat flux in three regions

Figure 4.6 presents a plot of heat flux, q, at different locations along *z*. Heat flux is defined as the rate of heat energy per unit area which transfers through water from a given wall surface in unit of W/m^2.

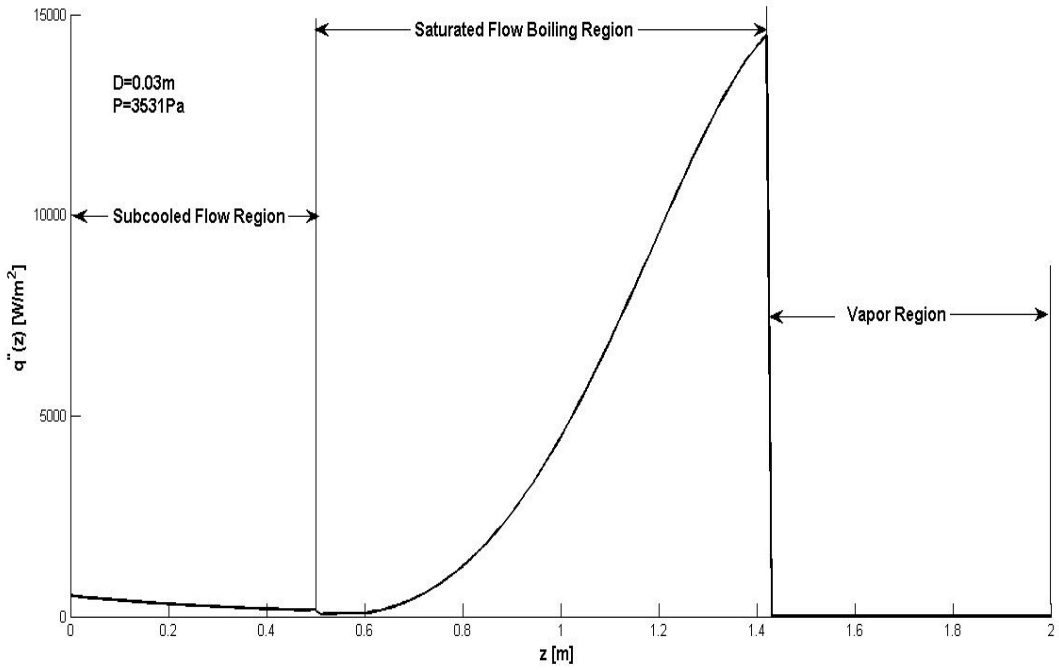

Figure 4.6 heat flux (W/m^2) in different regions versus *z*

In the Figure 4.6, the heat flux is dropping gradually from the water inlet along the subcooled flow region. The reason is because there is higher temperature difference between the inlet water and tube wall. Though the convective heat transfer coefficient gradually increases (as shown in Figure 4.3), this temperature difference is dramatically decreasing (as shown in Figure 4.1). Therefore, the heat flux in the subcooled flow region decreases based on Equation 3.1.

In the saturated flow region in Figure 4.1, the temperature difference between wall and water is a constant. As mentioned above, the dramatic change of heat transfer coefficient in this region and thus the heat flux from Equation (3.1) varies along the saturation region. The heat flux in the first of nucleate boiling dominant (*NBD*) region decreases and then in the convective boiling dominant (*CBD*) gradually increases up to the vapor region.

The heat flux in the vapor region gradually decreases because of the decrease of temperature difference between the wall and vapor (see Figure 4.1), though the heat transfer coefficient along the vapor region increases insignificantly (see Figure 4.5). To better show the vapor region plot in Figure 4.6, the heat flux along z is zoomed in on Figure 4.7. Heat flux decreases from 4.513W/m^2 at the beginning of vapor region to 4.099W/m^2 at the end of tube.

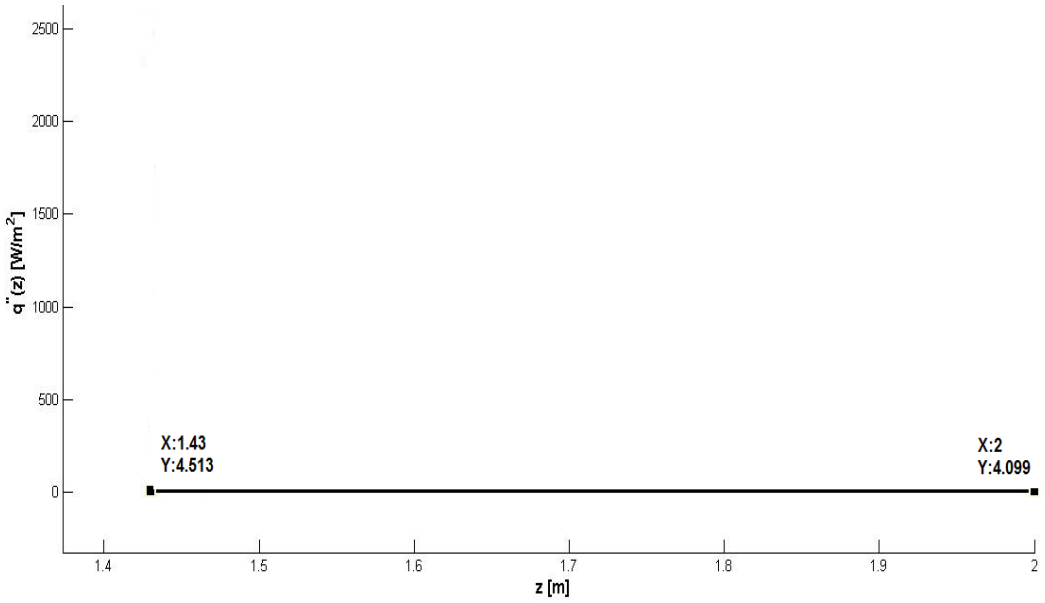

Figure 4.7 Vapor region graph with heat flux versus along tube length as coordinates

4.3.6 Analysis of heat transfer coefficient in different pressures

Figure 4.8 presents a plot of the heat transfer coefficient, h, along z with various pressure at 3,531, 2,617, 1,917 and 1,387Pa. The tube diameter and length are the same as 0.03 meter and 2 meter, respectively. Wall temperature stays constant at 302.6K.

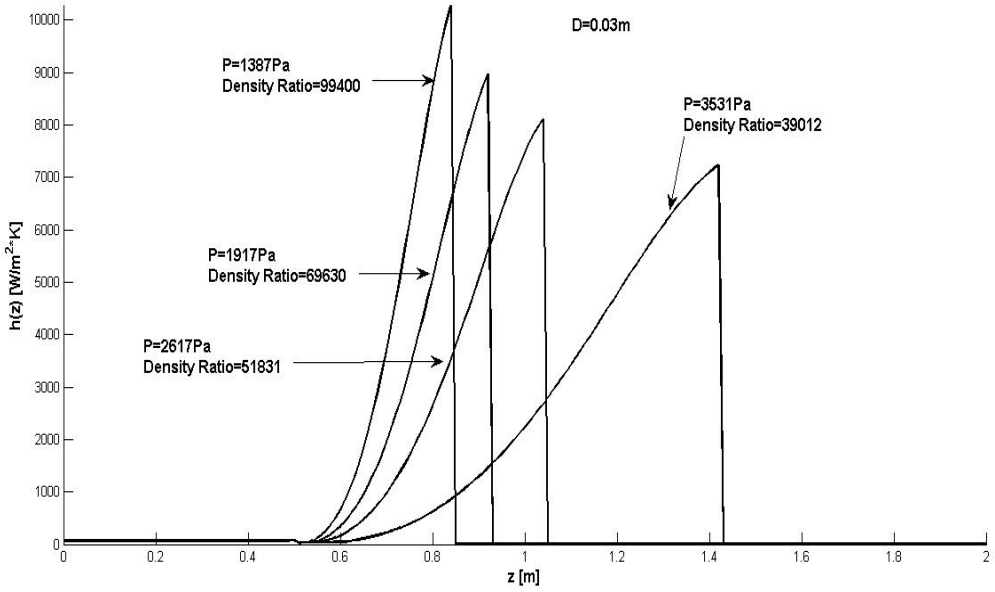

Figure 4.8 Heat transfer coefficient along *z* with various pressures

To better show the subcooled flow region plot, the subcooled flow region in Figure 4.8 is zoomed in on Figure 4.9. The variation of heat transfer coefficients at different pressures in the subcooled flow region is due to water inlet temperature to the tube and water thermal conductivity. Water saturation temperature decreases as pressure decrease. In this study, the water inlet temperature is set 5 ^{o}C below the saturation temperature to ensure pure water at the inlet. The water inlet and saturation temperatures at different pressures influences on the variation of the heat transfer coefficient (see Figure 4.10). As Figure 4.9 shows, the heat transfer coefficient is dependent on the temperature of inlet water and the pressure inside the tube.

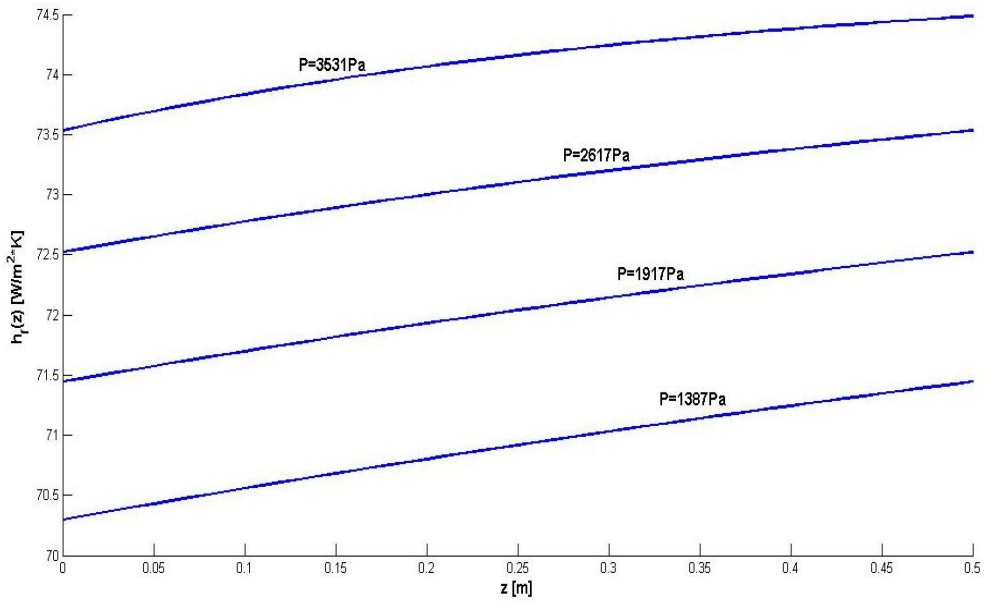

Figure 4.9 Heat transfer coefficient in subcooled flow region at different pressures

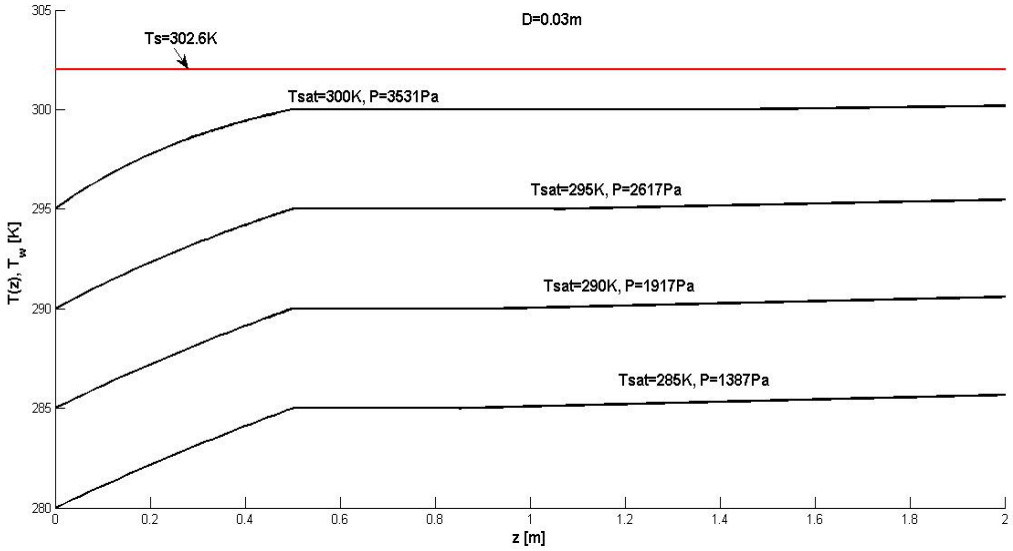

Figure 4.10 The temperature profile with different pressures; Tube diameter of 0.03m

In the saturated flow-boiling region, the slope of the upward trend of the heat transfer coefficient increases as the pressure increases as shown in Figure 4.8. As pressure decreases, the specific density of liquid increases and specific density of vapor decreases

(see Table 4.1). Therefore, the increase of liquid density increases the local convective heat transfer coefficient based on Equation (3.10) and (3.11). In these two equations density ratio ρ_l/ρ_g increases that will cause an increase of heat transfer coefficients.

At high pressure (such as 3531Pa), liquid boils at a higher temperature, so the nucleate boiling region has to be extended. The stronger and longer effect of the nucleate boiling region causes the less steep upward convective trend (see Figure 4.11).

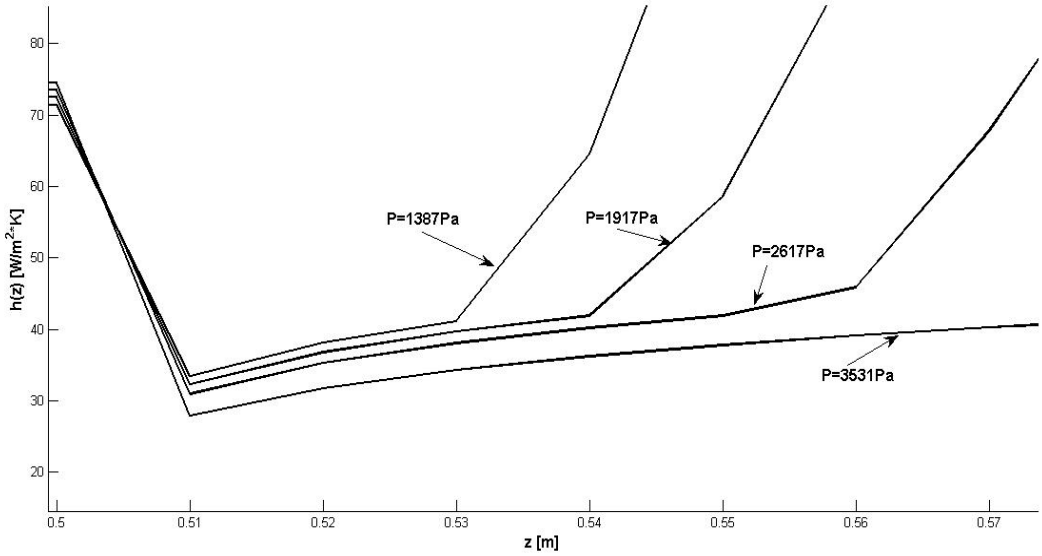

Figure 4.11 Effect of nucleate boiling dominant region in different pressures

4.3.7 Analysis of heat flux with different pressures

In Figure 4.12, heat fluxes with various pressures are shown. From Equation 3.1, the heat flux is related to the heat transfer coefficient. When the local heat transfer coefficient varies along the tube, the local heat flux along the tube also varies. Since the local heat transfer coefficient increases as pressure decreases along the tube in the saturation flow region, the local heat flux accordingly increases along the tube. From Equation 3.18, the total heat transfer rate $\dot{Q}(\mathrm{W})$ increases along the tube.

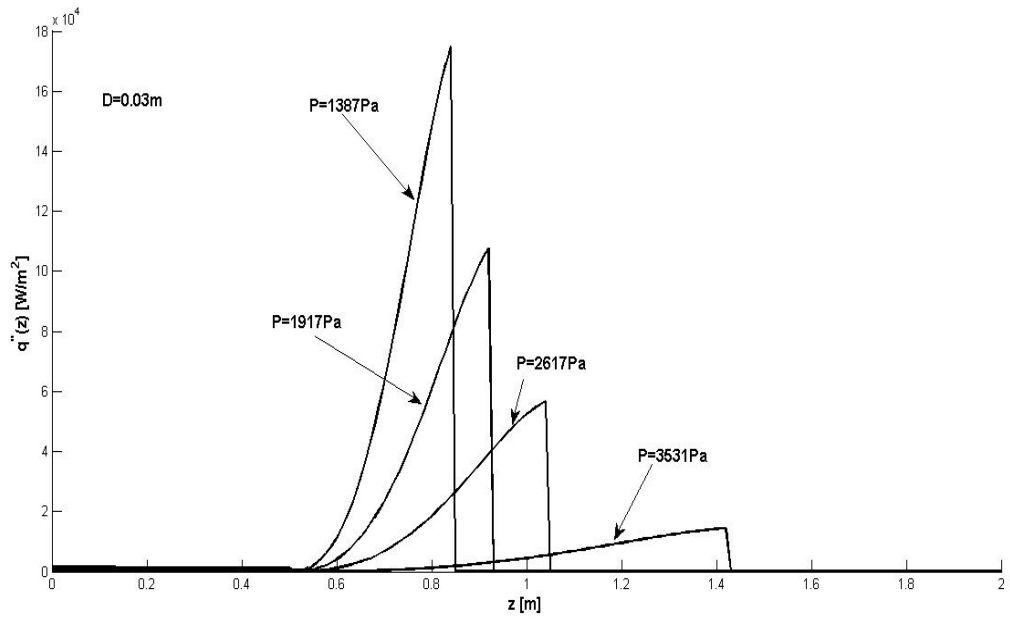

Figure 4.12 Variation of heat flux in different pressures

4.4 Experiments' Limitations

An experiment was set to verify the simulation results. The test rig, that is a system with boiling–condensing cycle, consists of a heat exchanger connected to fresh water supply (as shown in Figure 6.1) and was used to simulate the situation of a constant heat flux boundary condition. However, due to missing data and unsteady boiling flow, the exact mass flow rate entering to the tube cannot be determined. The steady-state is difficult to be reached in the boiling natural circulation loop as mentioned in Goswami *et al*. (2011). Kandlikar correlations are used for simulating heat transfer coefficient along the tube in our case study. The correlation model has been widely verified (Kandlikar *et al*., 1999) with past experimental data.

4.5 Summary

In this chapter, heat transfer coefficients and heat flux at different flow regions are analyzed based on a tube length of 2 m, tube diameter 0.03m, wall temperature of 302.6K, and different pressure consisting of 3,531Pa, 2,617Pa, 1,917Pa, and 1,387Pa. The plots of heat flux versus tube length in a specific tube diameter and different pressures are presented. In each region, the characteristics of properties and parameters on the heat transfer coefficient and heat flux are discussed and analyzed. Based on the analysis of heat transfer coefficient and heat flux, it is shown that the low pressure of 1387Pa among four pressures being considered is the best in terms of maximizing these two parameters. It is concluded that the total heat transfer rate in a solar collector tube at lower pressure should be increased with the proposed configuration. The next step of the analysis is to optimize the tube size to obtain a higher total heat transfer rate at a specific pressure.

Chapter 5

5. Optimization Estimation

5.1 Introduction

A series of parametric studies are conducted with the developed model to optimize the two-phase solar collector tube for a specific case study, i.e. at the average temperature of -8^{o}C in coldest months of Omaha, Nebraska. The parameters to be considered include the tube diameter, pressure, and tube length. The approach should be able to model the thermal behavior of the proposed system as a tool for design and optimization. The best tube size and pressure is discussed to maximize the total heat transfer rate through the tube for the possible average minimum temperature in Omaha, Nebraska.

Mappings of total heat transfer rate of a 2m-length tube with a diameter of 0.03m are carried out with various lengths of a subcooled flow region and at various pressures (3,531, 2,617, 1,917, and 1,317Pa). Also, heat transfer coefficients at various locations along the tube with another tube diameter and pressure are plotted. Different lengths of subcooled flow regions are considered in order to investigate the optimized length of subcooled flow region and to produce the maximum heat transfer rate.

5.2 Heat transfer rate based on variation of subcooled flow region in different pressures

In Figure 5.1, the heat transfer rate is shown based on change of the lengths of the subcooled flow region and pressures with a tube diameter of 0.03m. The length of subcooled flow regions considered consists of 0.3m, 0.4m, 0.6m, 0.8m, 0.9m, 1.1m, 1.2m, 1.5m and 2m, while the pressures are 3,531Pa, 2,617Pa, 1,917Pa and 1,387Pa. It is

assumed that inlet water temperature is 5 ^{o}C less than saturation temperature in each selected pressure. The wall temperature is 302.6K based on the average solar radiation in Omaha. The reason for selecting the pressures above is that their saturation temperature is less than the estimated wall temperature, e.g. 302.6K (see Table 4.1). Therefore, the wall temperature can boil the water inside the tube in these pressures.

The heat transfer rate, $\dot{Q}$(W), will be computed and plotted in a contour plot, with the pressure in axis Y and tube coordinate in axis X. As shown in Figure 5.1, the total heat transfer rate increases as pressure inside the tube decreases. However, as the subcooled flow region decreases, for example to 0.3m, a decrease of the heat transfer rate occurs (between 1m and 1.2m but not exceeding 1.2m). The reason for the lower heat transfer rate with the smaller subcooled region is because of a smaller mass flow rate (see Table 5.2). As shown in the figure, if the subcooled flow region extends over 1.2m at pressure of 1,387Pa, the heat transfer rate will decrease. It is because the 2m tube can only cover a part of the saturation flow boiling region where it has a higher heat transfer coefficient than when its length is smaller than 0.8 m. Wet vapor will be produced. Therefore, for a tube length of 2m, the best size for the subcooled flow region in order to get the highest heat transfer rate is in the range of 1m and 1.2m, which maximizes the subcooled flow and saturation flow region (In turn, minimize the vapor region). Table 5.1 shows the actual values of heat transfer rates in different tests presented above.

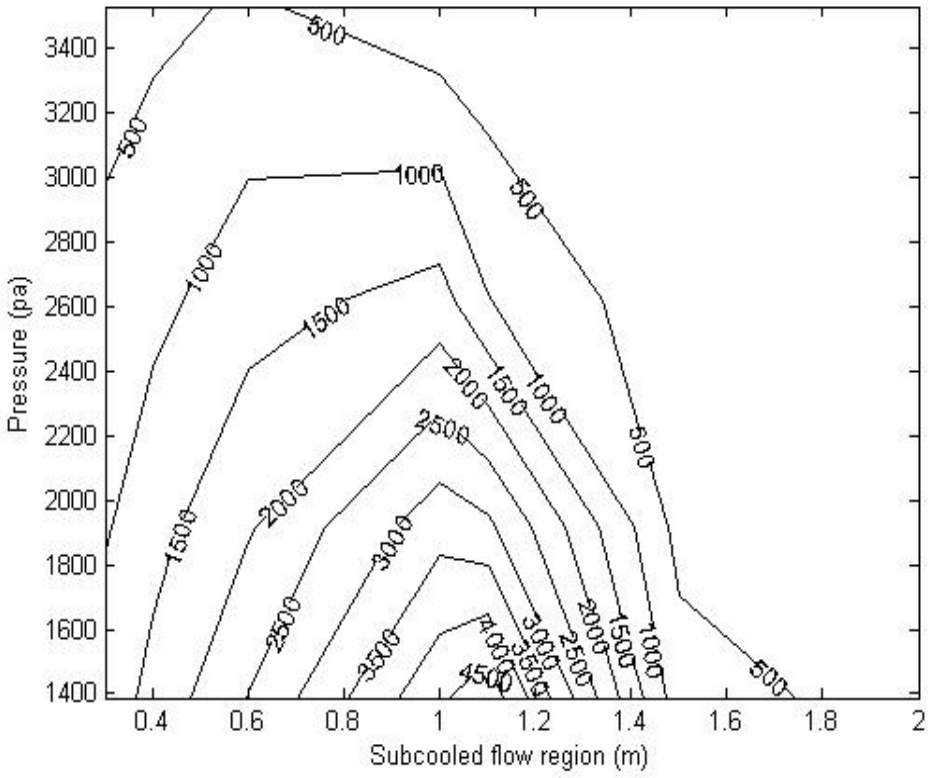

Figure 5.1 Heat transfer rate in a constant tube diameter (0.03m) with different pressures and length of the subcooled flow regions

Table 5.1 The total heat transfer rate in constant tube diameter

Pressure ***Subcooled Flow Region***	P1=3531Pa $\dot{Q}$(W)	P1=2617Pa $\dot{Q}$(W)	P2=1917Pa $\dot{Q}$(W)	P3=1387Pa $\dot{Q}$(W)
Z_{f1}=0.3m	280	645	957	1229
Z_{f2}=0.4m	380	867	1323	1660
Z_{f3}=0.6m	556	1307	1952	2522
Z_{f4}=0.8m	403	1749	2584	3553
Z_{f5}=0.9m	242	1970	2946	3983
Z_{f6}=1.1m	96	1019	3120	4845
Z_{f7}=1.2m	68	594	1844	4530
Z_{f8}=1.5m	60	154	344	732
Z_{f9}=2m	55	127	194	258

In the Table 5.2, the values of mass flow rate at different pressures with different subcooled flow regions are presented. At 3531Pa, as the subcooled flow region increases from 0.3 m to 2 m, the mass flow rate increases. Also, decreasing pressure from 3,531Pa to 1,387Pa with a fixed subcooled flow region, the mass flow rate increases due to reduced saturation temperature.

Table 5.2 Mass flow rate in constant tube diameter

Pressure ***Subcooled Flow Region***	P1=3531Pa $\dot{m}$(kg/s)	P1=2617Pa $\dot{m}$(kg/)	P2=191Pa $\dot{m}$(kg/s)	P3=1387Pa $\dot{m}$(kg/s)
Z_{f1}=0.3m	0.0004	0.000917	0.0014	0.0019
Z_{f2}=0.4m	0.0005	0.0012	0.0019	0.0025
Z_{f3}=0.6m	0.0008	0.0018	0.0028	0.0037
Z_{f4}=0.8m	0.0011	0.0024	0.0037	0.005
Z_{f5}=0.9m	0.0012	0.0028	0.0042	0.0056
Z_{f6}=1.1m	0.0015	0.0034	0.0051	0.0058
Z_{f7}=1.2m	0.0016	0.0037	0.0056	0.0074
Z_{f8}=1.5m	0.002	0.0046	0.007	0.0093
Z_{f9}=2m	0.0027	0.0061	0.0093	0.0124

5.3 Heat transfer rate based on variation of subcooled flow region in constant pressure

As shown in the Figure 5.2, the change of the subcooled flow region, □□, in overall tube length, with a constant pressure and a constant tube diameter affects the amount of total heat transfer rate in a solar collector. The goal of this section is to maximize the heat trasfer rate in a solar collector with a length of 2m and a diameter of 0.03m at a pressure of 1387Pa. The reason of choosing this pressure, i.e. 1,387Pa, is that the saturation temperature of the pressure is 285K and can transfer heat energy to the potable water

supply at a temperature close to 275K. However, one limitation of this system is that it may superheat the water and there will be a large vapor region at a higher tempratures. It may cause the system to be inefficient at over time. Any pressure under this specified pressure (1387Pa) is not a proper pressure for the design of a solar system because the saturation tempressure would be less than 285K which may not be enough to heat inlet water temprature. We should note that this system is designed and optimized for a specific case study, i.e. the average minimum temprature in the coldest months in Omaha, Nebraska. The optimization of the system for hot temperature, e.g. summer, is left for future study and it is outside of the scope of this study.

In the Figure 5.2, heat transfer coefficients are plotted along the tube. For maximizing the heat transfer rate, a tube with different initial subcooled flow region is considered in this figure for lengths varied from 0.3m to 2m. Referring to Figure 5.2, the best subcooled flow region is 1.15m which has a maximized heat transfer for this configuration. The vapor region that has the lowest heat transfer rate should be minimized. The saturated region which has the maximum heat transfer should be maximized. The subcooled region which governs the maximum mass flow should be maximized too. The Table 5.3 presents the value of the heat transfer rate along the tube with different subcooled flow regions.

For the case with a subcooled flow region larger than 1.15m, the vapor region would diminish and the saturation region will gradually decrease as the total length of pipe cannot cover the whole development of saturation flow boiling region. The reduction of the saturation region results in a decrease of heat transfer. That is why the heat transfer rate will eventually decrease after this point.

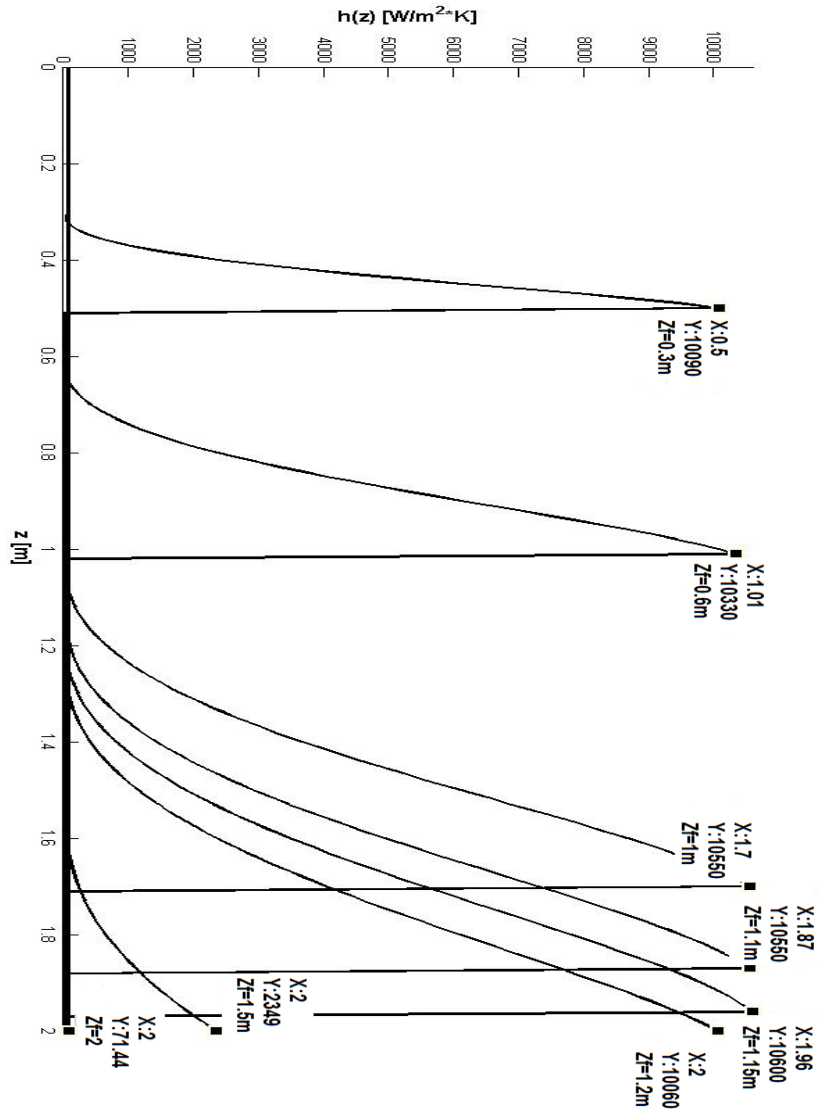

Figure 5.2 Different sizes of subcooled flow region to obtain maximum heat transfer coefficients; Pressure 1387Pa; Tube diameter 0.03m

Table 5.3 Total heat transfer rate in constant pressure, tube diameter of 0.03m

Subcooled Flow Region	***$\dot{Q}$(W)***
Z_{f1}=0.3m	1228
Z_{f2}=0.6m	2520
Z_{f3}=1m	4114
Z_{f4}=1.1m	4845
Z_{f5}=1.15m	5145
Z_{f6}=1.2m	4530
Z_{f7}=1.5m	732
Z_{f8}=2m	258

In the next case, the tube diameter is enlarged to 0.06m. In Figure 5.3, a plot is created for heat transfer coefficients along the tube with various length of the subcooled flow region. The condition of given data in this test is the same as the 5.3 section test, except that the tube diameter is 0.06m. The goal of this test is to compare the estimated total heat transfer rate with the change in diameter from 0.03m to 0.06m.

Table 5.4 presents the value of heat transfer rate overall for a tube length of 2m with different subcooled flow regions at a pressure of 1387Pa. The heat transfer rate increases as the subcooled flow region increases from 0.3m to 1.15m. When the subcooled flow region extended from 1.15m to 2m, the heat transfer rate decreases. Regard to the tube diameter change from 0.03m to 0.06m, the comparison of Figure 5.2 and Figure 5.3 shows that the heat transfer coefficient along the tube as the diameter decreases from 0.03m to 0.06m. But the comparison of Table 5.4 with Table 5.3 shows that the total heat

transfer rate obtained with a diameter of 0.06m is more than the tube with diameter of 0.03m.

Table 5.4 Total heat transfer rate in constant pressure, tube diameter of 0.06m

Subcooled Flow Region	$\dot{Q}$ ***(W)***
Z_1=0.3m	1263
Z_2=0.6m	2566
Z_4=1m	4466
Z_5=1.1m	4899
Z_6=1.15m	5200
Z_7=1.2m	4583
Z_{f8}=1.5m	746
Z_{f9}=2m	259

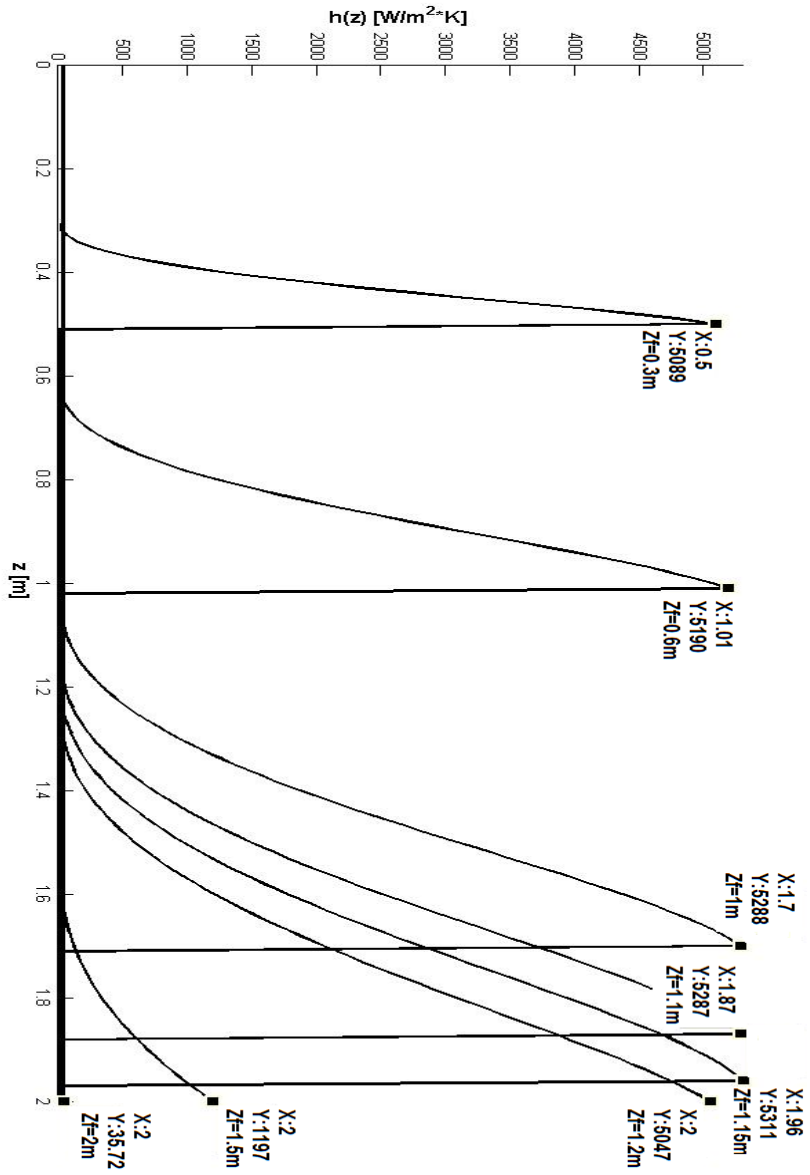

Figure 5.3 Heat transfer coefficients in different subcooled flow regions along a 2-m tube; Pressure 1387Pa; Tube diameter 0.06m

5.4 Summary

The objective of this chapter is to optimize the heat transfer rate in a case study of a low temperature, i.e. -8 ^{o}C, based on the variation of subcooled flow region along the tube at a pressure of 1,387Pa, to obtain a maximum heat transfer rate from a boiling-

condensing cycle. Generally, the maximum heat transfer rate occurs when the subcooled flow and saturations flow regions can be maximized and the vapor regions minimized. In the case of a 2m length pipe, the studies show that there is a specific length for the subcooled flow region that produces the highest heat transfer rate. This number is around 1m to 1.2m for a tube length of 2m. The heat transfer rate from the solar irradiation increases as the pressure decreases.

Chapter 6

6. Conclusion and Future Work

6.1 Summary

This study have investigated the heat transfer process and thermodynamic behaviors of fluid flow patterns of single and two-phase flow boiling in a black lacquer copper solar collator tube. A series of parametric studies were conducted to optimize a two-phase solar collector for a case study that considers the minimum surrounding temperature of -8^{o}C, which is the average minimum temperature of Omaha, Nebraska in the coldest months.

Optimization of the heat transfer rate and prevention of freezing in solar collector pipe depend on tube diameter, the length of subcooled flow region and pressure. A simulation model programmed in MATLAB was developed for system design and operation. The solar collector was exposed average daily solar irradiation of 4.5 kWh/m^2/day in Omaha. The tube surface temperature was calculated to be 302.6K.

The variation of local heat transfer coefficient and heat flux in subcooled flow region, saturated flow boiling region and vapor region were simulated in particular pressures with a fixed tube diameter. In chapter 4, the increase of thermal conductivity of water in the subcooled flow region and vapor flow region caused the convective heat transfer coefficient to increase for given pressure. However, heat flux decreases due to mild increases of convective the heat transfer coefficient and temperature difference, between the wall and water dramatically decreased. In the saturated flow boiling region, the two-phase heat transfer coefficient in the nucleate boiling dominant region decreased due to reduction of the nucleate boiling component and the small difference of density between

water and vapor. Also, the heat flux dropped due to a decrease of the heat transfer coefficient. After the nucleate boiling dominant region along the saturation region, there is a convective boiling dominant region in which the convective heat transfer coefficient increased due to an increase of vapor quality and a significant difference of density between water and vapor. The heat flux in this region dramatically increased because of an increase of the heat transfer coefficient. As presented in chapter 4, as pressure decreases inside the tube, the local heat transfer coefficient and local heat flux increases.

In Chapter 5 (System Optimization), a contour plot was presented for optimization of heat transfer rate in a solar collector. The tube diameter was considered 0.03m. Different initial subcooled flow regions from 0.3m to 2m with overall tube length of 2m and pressures at 3,531Pa, 2,617Pa, 1,917Pa, and 1,387Pa were considered too. The result showed that a high heat transfer rate happens in the lowest pressure when the subcooled flow region is in the range of 1 to 1.2m, with an overall tube length of 2m.

In chapter 5, the high heat transfer rate happens along the tube when the subcooled flow region is around 1.15m, while the saturation flow region and minimum portion of vapor region exist along the tube. Based on the results of this research, the optimum design for subcooled, saturation, and vapor region happens in the case where the subcooled flow and saturation flow regions are maximized, and the vapor region is minimized. In this case, the mass flow and heat transfer are maximized for subcooled and saturation regions, respectively. Therefore, the total heat transfer rate increases in the overall size of the tube.

6.2 Future work

There are several topics that can be expanded for the future research:

A. A solar collector can be designed in different weather conditions, and the thermodynamic behavior of two-phase system can be simulated. For example, in this research, the solar collector system is designed and optimized based on coldest months in Omaha, Nebraska with a surrounding temperature of -8^{o}C. However, if someone wants to use this system annually and optimize the heat transfer rate for all seasons, it is suggested that the system be designed and optimized for other surrounding temperatures. Designing the system with a higher surrounding temperature may increase the optimal pressure inside the tube. In this case, the water inside the tube may freeze in the coldest temperature, e.g. -8^{o}C More investigation about the optimal system in terms of annual energy saving can be done in future.

B. Other parts of the domestic water heating system, such as heat exchanger, water return pipe and condensate return pipe can be designed and investigated as future research. For example, the proper heat exchanger and the number of tubes needed in the system should be investigated more in future study.

C. An experimental case study can be developed to further study of the effectiveness of the proposed solar collector in improving the ability to save energy.

D. Cost-effectiveness and the payback period for a solar domestic water heating system that depends on the design, installation and consumption of energy can be investigated in future work.

E. As the primary research in this study, a test rig for testing a single pipe thermosiphon has been completed and a battery of tests conducted. A number of modifications to the original thermosiphon design were required for maintenance and testing purposes. A counter-flow valve was installed next to the flow meter in order to deal with cool down conditions after a test was run. Thermal insulation was installed on all exposed unheated pipe. Additionally, a drain valve was installed for maintenance purposes (see Figure 6.1). Several tests were conducted with a variety of constant heat flux conditions and data was gathered for each run. For future work, it is suggested that the heat transfer coefficient of this equipment be computed for different regions such as subcooled, saturation, and vapor in various pressures based on constant heat flux for verification.

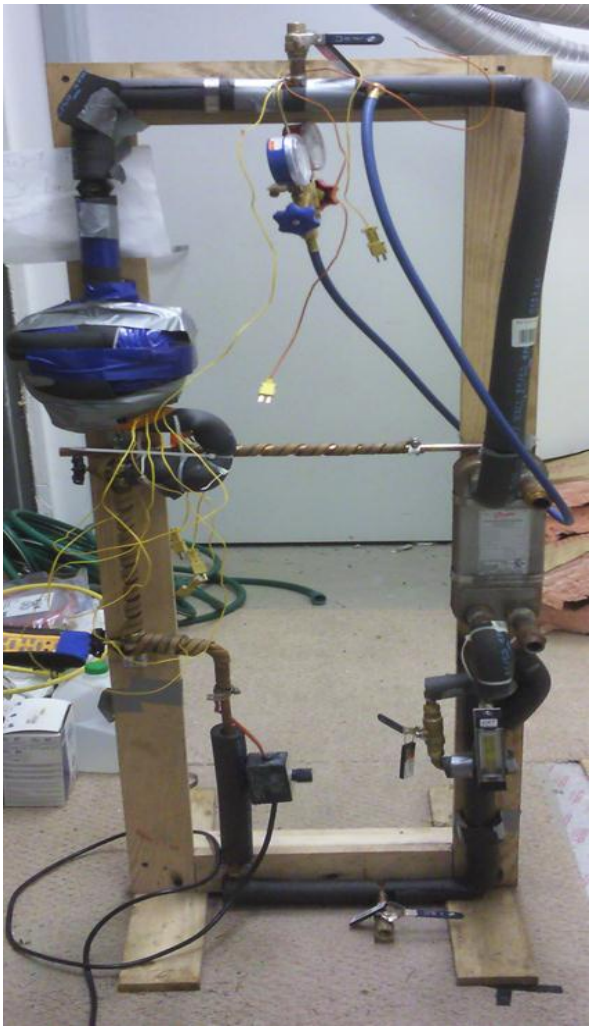

Figure 6.1 Test rig

7. References

[Anderson et al., 2009] William G. Anderson, Michael C. Ellis, and Kara L. Walker, "Variable conductance heat pipe radiators for Lunar and Martian environments," Proceedings of Space, Propulsion & Energy Science International Forum, (2009): 57–66.

[Collier and Thome, 1996] John G. Collier and John R. Thome, Convective Boiling and Condensation, Third Edition (Oxford University Press, 1996), 173.

[DOE, 2009]"Department of Energy (DOE), (accessed on August 6, 2010), http://www1.eere.energy.gov/ buildings/building_america/index.html.

[Esen and Esen, 2005] Mehmet Esen and Himket Esen, "Experimental investigation of a two-phase closed thermosyphon solar water heater, "Solar Energy, 79(2005): 459–468.

[Incropera et al., 2006] Frank P. Incropera, David P. Dewitt, Theodore L. Bergman, and Adrienn S. Lavine, Fundamental of Heat and Mass Transfer, 6th Edition,(John Wiley & Son, 2006) 638-640.

[Saffari and Ghobadi, 2010] Hamid Saffari and Mehdi Ghobadi, "Calculation of Convective Boiling in a Vertical Tube at Sub- atmospheric Pressures," Australine Journal of Basic and Applied Sciences, 4(2010):687-697.

[Shamsuzzoha *et al.*, 2004] M. Shamsuzzoha, M. Kamil, and S.S Alam, "Condition of Onset of Boiling in a Vertical Thermosiphon Reboiler," Journal of Thermophysics and Heat Transfer Vol. 18, No 4(2004).

[Hussein, 2007] Hussein, H.M.S., "Theoretical and experimental investigation of wickless heat pipes flat plate solar collector with cross flow heat exchanger", Energy Conversion and Management, 48(2007): 1266–1272.

[Hwang et al., 2007] Hwang, G.S., Kaviany, M., Anderson, W.G., and Zho, J,"Modulated wick heat pipe," International Journal of Heat and Mass Transfer, 50(2007): 1420–1434.

[Joudi et al., 1999] Joudi, K.A., Al-Tabbakh, A.A, "Computer simulation of a two phase thermosyphon solar domestic hot water heating system," Energy Conversion and Management, 40(1999):775–793.

[PV, 2010] James P. Dunlop, "Photovoltaic Systems" 2th Edition (in partnership with NJATC, 2010) 26-35

[Holman, 1992] Jack Philip Holman, Heat Transfer, 7th Edition, (Mc GrawHill, 1991) 471.

[Kandlikar, 1990] Satish G. Kandlikar, "A General Correlation for Saturated Two-Phase Flow Boiling Heat Transfer Inside Horizontal and Vertical Tubes," Journal of Heat Transfer, 112(1990): 218-228.

[Kandlikar, 1991] Satish. G. Kandlikar, "Development of a Flow Boiling Map for Subcooled and Saturated Flow Boiling of Different Fluids inside Circular Rubes," Journal of Heat Transfer, 113(1991):190-200.

[Kandlikar et al., 1999] Satish G. Kandlikar, Masahiro Shoji, V. K. Dhir, "Handbook of phase change boiling and condensation," (CRC Press, 1999) 366-397.

[Kincaid et al. 2002] Kincaid, D. Cheney, W., 2002. Numerical analysis: mathematics of scientific computing, third edition, Brooks/Cole, Pacific Grove, California.

[Kamil et al., 1995] Mohammed Kamil. H. Ali. S.S.Alam, "Heat Transfer to Boiling Liquids in a Single Vertical Tube Thermosiphon Reboiler," Experimental Thermal and Fluid Science, 10(1995): 55-53.

[MAT, 2010] "Matlab software," accessed November 20, 2011, http://www.mathworks.com/.

[IAPWS, 2007] "The International Association for the Properties of Water and Steam" accessed August 2007, http://www.iapws.org/relguide/IF97-Rev.pdf.

[NREL, 2008] "National Renewable Energy Laboratory Resource Assessment Program", accessed Octobert 2011, http://www.solar-estimate.org/solar_radiance.pdf.

[N.Goswami *et al*., 2011] N.Goswami, S. Paruya, 2011. "Advanced on the Research on the Nonlinear Phenomena in the Natural Boiling Circulation Loop," Progress in Nuclear Energy, 53(2011) 673-697.

[Ziadi et al., 2008] Sadaf Ziadi, M. Idrees, S.S. Alam, 2008. "Circulation Rates of Boiling Liquids in a Vertical Tube," Chemical Engineering Research and Design, 86, 499-507.

[TWC, 2012],"The Weather Channel, Omaha NE", accessed January 2012, http://www.weather.com/weather/wxclimatology/monthly/graph/USNE0363

[Wangee Chun et al., 1999] Wangee Chun, Yong Heack Kang, Hee Youl Kwak, Young Soo Lee, "An Experimental Study of the Utilization of Heat Pipes for Solar Water Heaters," Applied Thermal Engineering, 19(1999) 807-817.

[WIK, 2012]"Earth's energy budget" accessed January 2012, http://en.wikipedia.org/wiki/Earth's_energy_budget